Master's Theses and Doctoral Dissertations

Master's Theses, and Doctoral Dissertations, and
Graduate Capstone Projects

2005

Investigation of the optical, thermal, and mechanical properties of a bulk polymer using the surface thermal lensing technique

Bushra Hussain

Follow this and additional works at: http://commons.emich.edu/theses

Part of the Physics Commons

Recommended Citation

INVESTIGATION OF THE OPTICAL, THERMAL, AND MECHANICAL

PROPERTIES OF A BULK POLYMER USING THE SURFACE THERMAL

LENSING TECHNIQUE

By

Bushra Hussain

Thesis

Submitted to the Department of Physics and Astronomy

Eastern Michigan University

In partial fulfillment of the requirements

For the degree of

MASTER OF SCIENCE

in

Physics

August 23, 2005

Ypsilanti, Michigan

DEDICATION

To my Brother, Syed Intesar Hussain

ACKNOWLEDGEMENTS

I feel great pleasure to express my sincere gratitude to my thesis advisor Professor Marshall Thomsen for initiating this research topic and for his constructive criticism, encouragement, guidance, support, and patience throughout the length of this investigation. I would also like to thank Professor Donald Snyder of the Chemistry Department, who collaborated with Professor Marshall Thomsen, for his support and guidance whenever I needed it.

I thank the National Science Foundation for its partial funding to support the project. I also thank the Department of Physics and Astronomy for providing good research facilities.

I'm very grateful to my family for their moral support, especially my brother, Syed Intesar Hussain, for his technical and moral support.

My appreciations and thanks to all the committee members for taking the time to read my thesis. I also thank Dr. Kevin Kuehn of the Biology Department for allowing the use of the microscope in the biology lab.

Last but not least I would like to thank my co-worker Nandita Prasad for her cooperation and help in the initial set-up of the experiments.

ABSTRACT

The sensitive and simple photothermal technique of Surface Thermal Lensing (STL) was employed to study the thermo-mechanical response of an amorphous polycarbonate as a bulk. A discussion is given of how previously developed theories did not fit well with the present work. Therefore, only qualitative analysis and discussion of the experimental results is made, emphasizing the influence of various factors on the STL signal. The work here is mainly a study of the dependence of the STL signal on the modulated pump beam frequency. The effect on the STL signal of thermal and mechanical relaxation in the thermally stimulated area is also discussed qualitatively. Some normalization procedures were developed to show that most of the spots on the bulk polycarbonate sample followed a common trend and showed position dependence of optical, thermal, and mechanical properties of the sample.

TABLE OF CONTENTS

LIST OF FIGURES

Chapter 1: INTRODUCTION

Photothermal techniques were developed from photoacoustic spectroscopy[1] in the 1970s and are known for their nondestructive and noninvasive inspection of materials. These techniques have greatly developed and expanded over the last two decades. The basic process for the technique is called the photothermal effect. It is based on the principle of conversion of optical energy to thermal energy. When optical energy is incident on a sample, part or all of the energy is absorbed in the form of thermal energy. This absorbed energy causes localized changes in the sample. These changes are then detected by a probe to study various characteristics of the sample. The source of optical energy is usually a modulated laser beam, called the pump beam. The modulated beam may be in the form of short intense pulses separated by long dark periods (called pulsed-detection in time domain) or a continuous train of pulses at 50% duty cycle (called intensity modulated-detection in frequency domain). A second laser beam, called the probe beam, is used to detect the changes in the heated sample.

The versatility of photothermal techniques can be understood from their applications to a wide spectrum of materials, such as semiconductors[2], glasses[3, 4], biological specimens[5-7], polymers[8, 9], and ceramics[10]. These are applied to solids, liquids, and gases[11, 12], and opaque[13] and transparent[14] materials. These techniques are not limited to thin films and bulk samples but are applied to systems, such as interfaces[15] and multilayer samples[16, 17].

Nondestructive and non-contact inspection of these techniques makes them very useful and powerful tools for a broad range of applications. These include measurement of optical, thermal, and thermoelastic properties[11, 18-26], analysis of local defects[27-38], investigation of laser interaction dynamics[39-43], determination of laser damage thresholds[40-47], and monitoring contamination effects on optical components[48]. Some other interesting applications include determination of transport properties of multilayer superinsulation foils[17], which are used as thermal insulators for superconducting magnetic coils in particle accelerators, study of nonlinear absorption by melanin and associated safety implications[7], and inspection of thickness and defects in the coating of fabrics[14].

A large number of photothermal techniques have been developed over the last two decades[27, 49-54]. All of them can be used to characterize the absorption of materials by accurate, fast, in-situ and non-contact measurements. The most commonly used techniques are the photoacoustic method[22], the pyroelectric technique[22], photothermal calorimetery[55], photothermal reflectance[10,56], the photothermal deformation method[21,57-61], the mirage effect[12], the thermal lens technique[15, 62-65], and the surface thermal lensing technique[48, 66, 67]. Each method has its own characteristics that make it advantageous and disadvantageous in comparison with other methods. Hence the method used depends on the specific application. Some of the methods are discussed here briefly. The reader should refer to the references mentioned if further detail is required.

The photothermal deformation technique[60] is one of the most sensitive techniques. It was developed by Olmstead et al[60] in the early 1980s and was demonstrated to be an analysis tool for solid surfaces[68, 69]. It uses a modulated laser pump beam to heat the sample, and a very tightly focused probe beam is made to reflect from the deformation thus produced by heating. The reflected probe beam deflects from its original path due to the deformation; the amount of deflection is noted to find the slope of the deformation. It is used to measure the bulk thermal properties of optically flat materials[21, 60] and absorption in nonlinear optical films[61].

The mirage technique[12, 70], also known as the transverse photothermal beam deflection technique, detects the change in the refractive index of the air or gas adjacent to the surface of the sample. This change in the refractive index of the air is caused by the heated sample, which warms the air above it. Its sensitivity is less than the photothermal deformation method, but the signal modeling is simpler[71, 72].

Photothermal reflectance[10, 73-76] is similar to the photothermal deformation technique, except that here the probe beam is incident at the center of the heated area; therefore there is no angular deflection of the probe beam. This technique detects the change in the refractive index of the sample spot by measuring the amount of reflected radiation. The change in temperature causes change in refractive index, which, in turn, produces change in the amount of the reflected radiation. Its applications are limited to optical thin films. The photothermal reflectance technique is widely used for metals and semiconductors[56].

It is also used to measure thermal conductivity of dielectric thin film coatings with a metallic overcoat.

Another commonly used technique is the thermal lens[15]. It is a highly sensitive tool to determine thermo-optical properties of optical glasses[65], polymers[62, 64, 65] and liquids[63]. In this technique the pump and the probe beam are aligned colinearly. A localized change in the refractive index of the sample due to thermal heating produces a thermal lens that is then detected by the study of the focusing and defocusing of the pump and probe beam. Its sensitivity is lower than the photothermal displacement method, but its detection scheme is simpler.

To increase the sensitivity of the thermal lens technique, a promising new technique was developed by Kuo and his colleagues[66, 77, 78], called the surface thermal lensing technique (STL)[48, 66, 67, 70, 79-83]. Its sensitivity is demonstrated to be as high as the photothermal deformation technique, and the simplicity of the detection scheme is equal to that of the thermal lens technique. The experimental arrangement of the surface thermal lensing (STL) technique is similar to the photothermal deflection method except the probe beam diameter on the sample is greater than the pump beam diameter, which makes the beams' alignment much easier. Its high temporal resolution makes it a powerful tool for monitoring in real time the dynamics of the laser-induced change[70]. It is mostly applied to thin films and bare substrates[48, 66, 79]. Some of the work done so far on the STL technique is reported here. Krupka and Wu[48] studied the contamination effects on optical components. Wu and his colleagues[66] studied laser-induced surface deformation of thin

4

film coatings. Hu et al[67] used the STL technique to measure weak absorptance of thin film coatings. Yuan[25] and Bandi[26] studied the thermal mechanical properties of polymer thin films using this technique.

Work reported in this thesis is focused on the characterization of a bulk polymer sample using the STL technique. As already mentioned, the STL technique has been recently developed[80] and has proved to be a very promising technique for photothermal characterization of optical materials, especially weakly absorbing thin film coatings and bare substrates[48, 66, 79]. Its lower sensitivity to the environment makes it easier to handle where hostile environmental conditions are present. This characteristic makes it more practical for industrial applications. It can also be used to study details of non-linear behavior of optical thin films[61]. Fig. 1.1 depicts the principle of the STL technique.
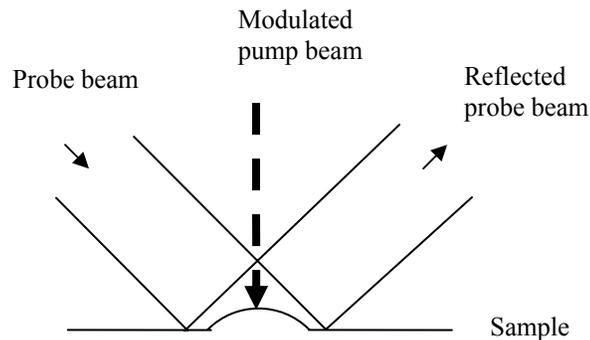
Fig. 1.1 Principle of Surface Thermal Lensing technique.

When a pump laser beam irradiates the surface of the sample, some of the optical energy is absorbed in the form of thermal energy, which then produces localized deformation of the surface due to thermal expansion. This deformation, called a thermal bump, behaves

as a curved reflection mirror. To detect thermal expansion of the thermal bump, a second laser beam, the probe beam, is focused on the bump (shown in Fig.1.1) with a larger diameter than the pump beam diameter. The probe beam reflected from the deformed area contains a diffraction pattern, which is used to measure the surface deformation or surface thermal lens. A CCD-camera can be placed in the path of the reflected probe beam, to image the whole beam profile, detecting any change in the probe beam profile. This detection method could be used if the photothermal signal is strong enough. But if the signal is not strong, then a pinhole detector is used to monitor the intensity of the central maxima of the diffraction pattern present in the reflected probe beam. To monitor the central intensity, the pump beam is chopped to produce a modulated central intensity, which is then monitored by a lock-in-amplifier. This modulation significantly increases the signal-to-noise ratio.

Much research has been carried out on polymers using various photothermal techniques because polymers are becoming very popular in industry and everyday applications. Polymers are widely used as structural materials because of the combination of their properties, such as low density, easy fabrication, good tensile strength and impact resistance. In agriculture, they are used for greenhouse structures because of their high optical transmittance. In the textile industry, they are used to make a number of different fabrics because of their elastic properties and durability. They are used in the food industry for packaging and in the automobile industry as coatings. Hence a very wide range of applications have been discovered, and further research is conducted to improve and enhance their use. Since some of these materials are weak absorbers in the optical

range, photothermal techniques (which can be very sensitive) have been found to be useful for the study of their optical properties and their response to any changes in the surroundings, such as contamination.

Some of the important work investigating polymers using photothermal techniques is discussed here. Rajasree et al[58] studied the laser-induced damage threshold for bulk polymers. Zambrano-Arjona et al[84] studied the charge recombination in organic polymeric semiconductors. Photothermal responses in opaque thin polymeric films were studied by deFreitas[13]. Einseidel et al[59] determined the order parameter C_2 in laser-beam-oriented polymer systems using the photothermal beam deflection technique. Rohling and colleagues studied the temperature dependence of thermo-optical properties of polymers such as polycarbonate[64]. Thermal properties of conducting polymers were obtained using photopyroelectric and photoacoustic spectroscopies[22]. Absorption measurements on nonlinear optical polymeric systems were made by Skumannich[61]. Ogawa et al[21] measured out-of-plane thermal diffusivity in free-standing polymer thin films, whereas Hu and his colleagues[16] carried out the same work on a wafer. Yuan[25] and Bandi[26] studied the thermal mechanical properties of polymers using the STL technique. Hence a large variety of work has been done on polymers using photothermal techniques.

From the references for the STL technique mentioned earlier in this chapter, one can conclude that most of the work on the STL technique has been applied to optical films. A literature search suggests the work reported in this thesis, the study of bulk polymers using the STL technique, is the first of its kind. The polymer used in the present work is

an amorphous bis-phenol A polycarbonate. Its versatility can be seen from its numerous applications such as in the automotive industry, medical and health care, bottles and packaging, household appliances, glazing and many more. This makes it a very important and popular material for investigation and characterization.

Previous work using STL techniques on inorganic films proved its ability to study local properties of the films. When the STL technique was first applied to polymer films, results seemed to indicate a significant variation from site to site of these local properties, demonstrating position dependence of the optical, thermal, and mechanical properties of thin polymer films. The results also showed variation in the STL signal intensity with the chopped pump beam frequency, which can be correlated to the thermo-mechanical properties of the sample. These preliminary results also showed significant time-dependence in the STL signal. The purpose of this work is to look for similar behavior in bulk polymers.

Chapter 2: THEORY

Various models and theories have been developed so far on the STL technique. A detailed study of these models and theories shows that some of the assumptions made to develop them do not fit well with the technique in this thesis, such as the geometry of the setup, so none of them can be used to analyze the data obtained in this thesis. Therefore, in this chapter a reasonable effort is made to interpret and understand qualitatively the influence of various factors on the STL signal. First, the importance of these factors is discussed and then their effect on the signal is analyzed. To begin the discussion, the concept of thermal waves is introduced, and its importance and effect on the STL signal are discussed.

Thermal Waves

The concept of thermal waves was introduced by Angstrom who, in 1861, described their use for the measurement of thermal diffusivity of materials. When a light beam is incident on a sample surface, the optical energy absorbed by the sample causes localized heating. In most photothermal experiments the light beam is modulated, which produces a time-dependent heat source. This time-dependent heat source leads to time-dependent temperature fields in the material and its surrounding media, due to the conduction process in the material. These changing temperature fields are referred to as thermal waves.

To describe mathematically the heat conduction process in a homogeneous and uniform solid state material, the thermal diffusion equation is given below:

$$\nabla^2 T(\mathbf{r},t) = \frac{1}{D}\left(\frac{\partial T(\mathbf{r},t)}{\partial t}\right) \quad \dots\dots\dots\dots\dots\dots\dots\dots\dots\dots\dots\dots\dots\dots\dots \text{(2.1)}$$

where $D = k(\rho c)^{-1}$ is thermal diffusivity, k, ρ, and c are the thermal conductivity, the density, and the specific heat, respectively, of the material.

The solution to the thermal diffusion equation when the heat source is periodic in time gives the relation for thermal waves. In a one-dimensional case, as shown in Fig 2.1, where a periodic heat source with the angular frequency ω is incident on the sample surface, the thermal wave can be expressed in the form

$$T(\mathbf{r},t) = T_o e^{-x/\mu} \cos\left(\frac{2\pi x}{\lambda} - \omega t\right) \quad \dots\dots\dots\dots\dots\dots\dots\dots\dots\dots\dots\dots\dots \text{(2.2)}$$

where μ is the thermal diffusion length defined as

$$\mu \equiv \sqrt{\frac{2D}{\omega}} \quad \dots\dots\dots\dots\dots\dots\dots\dots\dots\dots\dots\dots\dots\dots\dots\dots\dots \text{(2.3)}$$

and λ is the thermal wavelength, $\lambda \equiv 2\pi\mu$.

Eq. (2.2) shows that a thermal wave has two important characteristics. The first one is that it is heavily damped. The amplitude of a thermal wave decays exponentially when it propagates, where the thermal diffusion length μ determines the rate of decay of the thermal wave as it penetrates into the sample. Because the diffusion length is inversely

proportional to the square root of the frequency, the penetration depth of the thermal

wave decreases with increasing frequency[70].
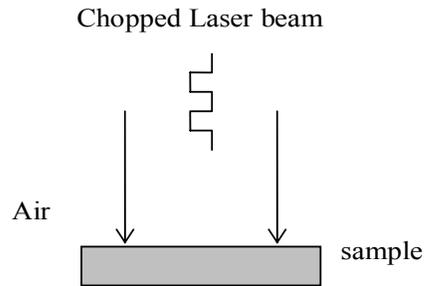
Fig. 2.1 A modulated beam generates a time-dependent temperature field in the sample.

The second characteristic of a thermal wave is that it is very dispersive, with its

propagation velocity υ strongly dependent on frequency,

$$\upsilon = \omega(\frac{\lambda}{2\pi}) = \sqrt{2\omega D} \quad \dots\dots\dots\dots\dots\dots\dots\dots\dots\dots\dots\dots\dots\dots\dots\dots\dots\dots\dots\dots\dots\dots\dots\dots\dots\dots(2.4)$$

Increasing the frequency will then lead to an increase in thermal wave velocity for a

given thermal diffusivity.

The combination of the above two features makes thermal waves important for

characterizing bulk samples. These features can be used for depth profiling of the

samples.

The penetration depth of the thermal wave at different frequencies can be evaluated. The velocity of the thermal wave at a certain modulated frequency can be calculated from Eq. (2.4), with the thermal diffusivity D characteristic of the material taken as constant. During each cycle, the beam is shut off half of the time. Therefore the time for which the beam is chopped is $t = (2f)^{-1}$. Multiplying t by its corresponding velocity results in a distance the thermal wave travels into the sample. It determines how deep the thermal wave penetrates before another wave is generated.

Factors Affecting the STL signal

There are a number of factors that influence the quality and magnitude of the STL signal. These factors are discussed briefly below.

Laser Intensity

Gaussian beams are defined as having a Gaussian intensity profile with a spot radius of w, which means the intensity of the beam reduces by a factor of e^2 (=7.389), with respect to the value at its centre, at a lateral distance of w from the axis of propagation. Then, w is called the spot size of the Gaussian beam. When a pump beam with a Gaussian intensity profile is incident on a sample spot, it would produce a Gaussian thermal bump if no thermal diffusivity were present. But since thermal diffusivity is never zero, the shape of the thermal bump will be modified.

The intensity of the pump beam in STL experiments helps determine how much energy is absorbed by the sample spot. The greater the intensity of the pump beam, the greater is

the amount of energy absorbed at a given optical absorptivity. This increased amount of energy absorbed increases the size of the thermal bump as well as its curvature, which is verified by the increased signal amplitude with intensity. If all of these processes are linear, the intensity of the pump beam has a linear relationship with the signal amplitude[60].

Optical Absorptivity

Optical absorptivity of a material is defined as the fraction of the incident radiation absorbed. Its value depends on the temperature of the material, the wavelength of the incident radiation, and on the material itself.

The STL signal mainly depends on how much energy a sample absorbs in each pulse. The greater the absorptivity, the greater is the fraction of energy absorbed by the sample spot, thus increasing the size of the thermal bump and therefore its curvature. Hence absorptivity is directly related to the magnitude of the signal. Any model predicting the STL signal may not have only the absorptivity or only the intensity in its relation, but rather the product of absorptivity and intensity is expected to be present in the relations. So if the signal is linear in intensity, it is linear in absorptivity.

Thermal Diffusivity

In heat transfer analysis, the ratio of the thermal conductivity to the volumetric heat capacity is an important property termed the thermal diffusivity

$$D = \frac{k}{\rho c}$$ …………………………………………………………….. (2.5)

13

where thermal conductivity is the rate at which thermal energy is transferred per unit area (perpendicular to the direction of propagation) per unit change in temperature. Thermal diffusivity measures the ability of a material to conduct thermal energy relative to its ability to store thermal energy. Materials of large thermal diffusivity will respond quickly to changes in their thermal environment, while materials of small thermal diffusivity will respond more sluggishly, taking longer to reach a new equilibrium condition.

This transport property plays a very crucial role in describing the size and thermal relaxation phenomenon of the bump generated on the surface of the sample. Smaller thermal diffusivity means more concentrated energy of the sample spot as compared to that for larger thermal diffusivity values. If the rest of the properties are assumed to be constant for a given sample spot, then for low thermal diffusivity the height of the thermal bump rises to a higher value than that for high thermal diffusivity, because lower thermal conduction results in greater thermal energy storage. For high thermal diffusivity, the thermal bump may be broader and less high.

Thermal diffusivity of the sample spot also affects thermal relaxation of the bump when the beam is blocked. Higher thermal diffusivity will cause the bump to relax more rapidly than lower thermal diffusivity because energy diffuses quickly through the sample.

A qualitative description of the phenomenon mentioned above is given as a graphical representation in Figs. 2.2(a), (b), and (c).
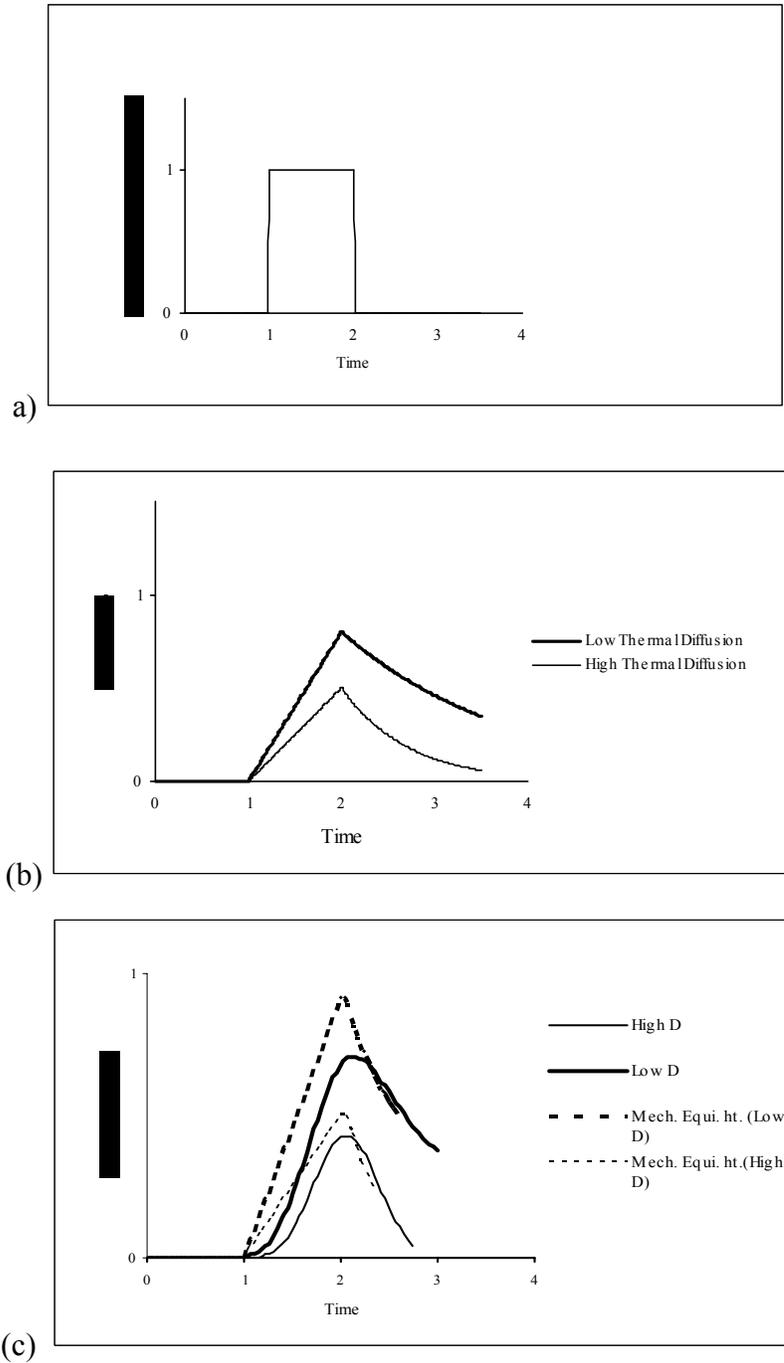
Figs. 2.2 (a) Chopped pump beam intensity versus time. (b) Schematic representation of the variation of temperature with time in response to the chopped pump beam at low and high thermal diffusivity. (c) Variation of mechanical bump height with time in response to the temperature variations at low and high thermal diffusivity. The dotted curves show the mechanical equilibrium heights (see text). All units are arbitrary.

A chopped pump beam is made to hit a sample spot, shown in Fig. 2.2(a). The instant the pump beam is incident on the sample spot, its temperature starts rising due to absorption of optical energy and conversion into thermal energy. The temperature keeps rising constantly while the beam is hitting the spot, Fig. 2.2(b). The moment the pump beam is chopped, the temperature starts falling exponentially. The rate of rise and fall of temperature depends on the spot's thermal diffusivity. At low thermal diffusivity, less heat diffuses out from the exposed spot during the time for which the beam is incident than at higher thermal diffusivity. Therefore, for a spot with low thermal diffusivity, the temperature rises to a higher value, just before the beam is chopped, than for a spot with high thermal diffusivity. When the pump beam is chopped, the temperature drops more rapidly for high thermal diffusivity than for low thermal diffusivity.

The increase in temperature causes thermal expansion depending on the spot's coefficient of thermal expansion, which in turn causes it to expand mechanically. The mechanical expansion is not instantaneous. Instead, there is a time lag due to the viscoelastic behavior of the sample spot[87] as seen in Fig 2.2(c). A qualitative description of the phenomenon is represented by the curves that refer to two different thermal diffusivities. The slope of the curve is steeper for low thermal diffusivity than for higher thermal diffusivity. The dotted curve represents the *mechanical equilibrium* bump height. It shows the height of the bump at each temperature when that temperature is maintained for a sufficient time to attain mechanical equilibrium. In fact, the spot does not reach mechanical equilibrium at any instant because of the constant rise in temperature. Therefore the bump height is always less than the equilibrium bump height. The instant

the pump beam is chopped, the mechanical equilibrium bump height starts to drop. The rate of the drop depends on the rate of fall in temperature, in other words, on the thermal diffusivity of the spot. The actual mechanical bump height does not start to decrease instantaneously but keeps building up due to the time lag. Thus the increase in bump height lags behind the temperature. As a result, the bump is still growing as the temperature first begins to drop. So the rate of increase in the height decreases till it reaches an equilibrium height. This is the point where the mechanical equilibrium bump height crosses the actual bump height. Beyond this point it is plausible that initially there is a gradual decrease in the height and then an exponential decay. A curve with low thermal diffusivity Fig 2.2(c) decays slowly. If the pump beam is blocked for a long enough time, then the two curves with the same thermal diffusivity, one representing mechanical equilibrium height and the other displaying the actual mechanical height, may coincide before the next part of the cycle starts.

In the case of a spot with higher thermal diffusivity, the bump reaches a lower height in the same time interval compared to when the pump beam is incident on a sample spot with low thermal diffusivity. When the beam is chopped, the bump takes less time to reach the mechanical equilibrium height or the crossover point, and afterwards the bump decays quickly. Since, at a given frequency, time lag is proportional to the phase lag between the input pump beam signal and the output STL signal, the phase lag is thus greater for a low thermal diffusivity spot than for a high thermal diffusivity spot.

The greater the relaxation time, the greater the phase lag between the two signals.

The relationship between the phase lag and the time lag is given as

$$\varphi = -\frac{T_L}{T_{ch}} \times 360 = -T_L \cdot f_{ch} \times 360 \quad \dots\dots\dots\dots\dots\dots\dots\dots\dots\dots\dots\dots\dots\dots \text{(2.6)}$$

where φ is measured in degrees, T_{ch} is the time period of the chopped pump beam,

and f_{ch} is the corresponding chopping frequency. The minus sign is added because T_L

refers to how much the STL signal lags behind the pump beam.

The above relationship suggests that the negative value of the phase lag may increase

linearly with the chopping frequency. However, if T_L itself depends on the chopping

frequency, then the relationship will not be linear.

Coefficient of Thermal Expansion

The coefficient of thermal expansion α_{th} is the fractional increase in the dimensions of a

material through one degree rise in temperature. This quantity determines the mechanical

response of the sample spot. A larger thermal expansion coefficient causes greater

expansion per degree rise in temperature, generating a bigger size bump as compared to

when α_{th} is small. Hence there exists a linear relationship between the size of the bump

and the coefficient of thermal expansion.

Elasticity (Elastic Modulus)

Elasticity is the ability of a material to come back to its original shape and size once a deforming stress has been removed. It is characterized in part by the material's elastic modulus.

The elastic modulus is defined as the ratio of stress to strain.

$$E = \frac{\sigma}{\varepsilon}$$ …………………………………………………………. (2.7)

where σ is the applied stress and ε is the strain thus produced.

On an atomic scale, macroscopic strain is manifested as small changes in the interatomic spacing and the stretching of interatomic bonds. As a consequence, the magnitude of the modulus of elasticity is a measure of the resistance to the separation of adjacent atoms, that is, of the interatomic bonding forces[85].

The value of the modulus depends on the amount of stress applied, the time for which it is applied, the temperature and the nature of the material. The greater the modulus, the smaller the strain produced by a certain amount of stress. Hence a higher modulus will result in a smaller bump.

The duration of the stress applied also affects the modulus [86]. With the increase in time for which stress is applied, the modulus of the material decreases, making it softer. At lower chopping frequencies, the pump beam is incident on the sample for a longer period

19

of time, thus decreasing its modulus. But at higher frequencies the exposure time is reduced, causing less decrease in its modulus. This effect will tend to produce a bigger bump at lower frequencies than at higher ones.

A material's deformation response to the applied stress is an important factor in determining the phase lag between the input and the output signal. These deformation responses are classified as[87]

1.   Instantaneous elastic deformation (reversible)
2.   Time-dependent viscoelastic deformation or relaxation (reversible)
3.   Time-dependent viscous deformation (irreversible)

In a reversible elastic deformation, the material responds instantaneously to the applied stress and returns instantaneously to its initial state when the stress is removed. Hence no phase lag between the stress and the strain signal is observed for a purely elastic material.

The time-dependent reversible viscoelastic deformation is positioned between elastic and viscous deformations. In this case, the material does not instantaneously respond to the applied stress; some relaxation time is required to reach an equilibrium state. When stress is removed, the material returns to its initial equilibrium state after that relaxation time. The relaxation time τ is defined as "the time-dependent tendency of the material to reach an equilibrium state when externally loaded"[87]. It is obtained from the viscous and the elastic response of the material.

$$\tau = \frac{\eta_{rel}}{E_{rel}} \quad \text{...} \quad (2\text{-}8)$$

where η_{rel} is the viscosity and E_{rel} is the modulus.

The third deformation response is also time-dependent, but it is irreversible. The material under stress starts flowing and never returns to its initial equilibrium.

The most intriguing deformation response contributing to an STL signal is the time-dependent reversible viscoelastic deformation response. When a periodic stress is applied to a material, a periodic strain with a phase shift is produced with respect to the phase of the stress signal due to this time-dependent behavior. The relationship between time lag and phase lag is governed by Eq 2.6.

If the relaxation time is greater than the time for which the pump beam is chopped, the bump never relaxes completely. On the other hand, the bump may relax completely if the relaxation time is less. At lower frequencies, the beam is chopped for a longer period of time, so for a given relaxation time the bump may relax more or even completely at lower frequencies while it is unable to relax at higher ones.

Pump Beam Chopping Frequency

A modulated or chopped pump beam is one of the requirements for the STL technique. The frequency of the chopped pump beam (the chopping frequency) also affects the STL signal. The chopped beam propagates in the form of square waves. At low frequencies

the pump beam stays on and off for a longer period of time than at high frequencies. Therefore, the sample is exposed to the pump beam for a longer time and thus absorbs more energy at lower frequencies. This difference, at low and high frequencies, in the time duration for which the beam is incident on the sample and for which it is stopped causes variation in certain quantities of the sample spot, such as thermal diffusion length, amount of energy absorbed, and velocity of thermal waves. The thermal diffusion length and the thermal wave velocity were already discussed earlier in this section, but the energy absorbed requires discussion. Because the amount of energy directly depends on the time the pump beam is incident on the sample during one cycle, and the STL signal is proportional to the amount of energy absorbed, the STL signal should be inversely related to the pump beam chopping frequency if the only factor responsible for the STL signal were the amount of energy absorbed.

Characteristics of Probe Beam

The probe beam is used to reveal any changes on the sample spot produced by the pump beam, without causing an effect of its own on the sample. Hence it is essential to discuss the effects of its characteristics on the STL signal. There are a number of characteristics that need consideration in this respect, most critical of which are its intensity, wavelength, diameter, and angle of incidence with respect to the surface of the sample.

 Intensity of the Probe Beam   The intensity of the probe beam is important in this regard because a too intense beam may result in significant absorption by the sample spot,

producing a thermal bump of its own. This bump will then overlap with the bump created by the pump beam, producing data that are hard to interpret. On the other hand, if the beam is too weak (very low intensity) it will not be possible to obtain a signal that is detectable by the lock-in amplifier. Hence a reasonable intensity of the probe beam must be chosen.

Wavelength of the Probe Beam   The wavelength of the probe beam affects the absorption of the beam by the sample. Absorptivity is known to depend on the wavelength of the incident radiation. Polymers are found to be minimally absorptive in the visible range, so the wavelength of the probe for a polymer experiment should be chosen to lie in the visible region to reduce its absorption.

Diameter of the Probe Beam To produce an STL signal, the diameter of the probe beam should be greater than the diameter of the pump beam. A smaller diameter will not completely overlap the pump beam spot, and it may produce a deflection signal instead of diffraction if the diameter is very small in comparison to the pump beam diameter. A too large spot is also not a good choice because most of the reflections of the probe beam will occur from the flat surface instead of just from the surface thermal lens. The spot size of the probe beam must be such that the reflections are mostly from the thermal lens generated by the pump beam and it must enable easy alignment.

Incident Angle of the Probe Beam The incident angle is the angle the probe beam makes with the normal to the sample surface. The incident angle also affects the overall signal.

No useful information is yet known for the optimum angle of incidence. Therefore the choice is simply based on geometric constraints of the set up. Some theories and models assume an incident angle of 0°, but geometrically it is not possible to set up the pump beam, the probe beam, and the detector at the same location. Even if it is possible, then unwanted multiple reflections from the pump and the probe will enter the detector and overlap the actual signal.

General Theoretical Models

Various models for thermal lensing techniques have been developed so far. The first theoretical model for the detection of a thermal lens was presented by Gordon [88]. In this model, a single laser beam was used to relate the focal length of the thermal lens with the thermo-optic properties of the medium, using the assumption that the variation in the refractive index is parabolic about the beam axis. Later, with the same parabolic profile for the refractive index, Hu and Whinnery *et al* [89] derived a model that related the changes in the beam center intensity and spot radius to the absorption coefficient of the sample. Their theory was then extended by Twarowski and Kliger [90], where pulsed mode laser thermal lens effect measurements were made. Gordon *et al's* theory was extended by Sheldon *et al* [91], where the Fresnel diffraction model was used to take into account the effects of aberrations in the lens. These aberrations were introduced by the deviation in the thermal profile from its assumed ideal parabolic profile. All these models mentioned above, except that of Twarowski and Kliger, use a single beam for both pump and the probe, but later work is more focused on dual beam pulsed mode thermal lens detection, which is the technique presented in this thesis[77,92,93]. In this method, first a pulsed beam is

used to heat the sample and the second beam, the probe beam, is used to detect the lens formation.

Power[93] developed a model based on the dual beam detection method. This model enabled the computation of the entire probe beam intensity profile for the detection of the thermal lens formed in a liquid and the measurements of the absorption coefficient of the sample. It also accounted for the thermal lens aberrations using the Fresnel diffraction model. In this model the thermal lensing technique (Chapter 1) is used, which is related to but not identical to the technique used in this thesis.

STL Theoretical Model

A more closely related model to the work in this thesis was developed by Kuo[77]. It presents a sensitive interferometric technique used to measure the thermal bump produced by an intensity-modulated pump beam and detected by the probe beam. The reflected beam contains a diffraction pattern that gives information about the thermal bump, called the surface thermal lens, and extracts information about the thermal, optical, and elastic properties of the sample. The technique is thus called the Surface Thermal Lensing technique.

To develop this model, Kuo assumed that the height of the thermal bump has a Gaussian profile and the entire bump has a spatially uniform phase. These two assumptions are reasonable if the thermal diffusion length is much smaller than the radius of the heating

beam and if there is no viscoelastic response in the sample. With these conditions, the thermal bump size barely exceeds the size of the heating beam.

Other assumptions are related to the geometry of the setup. In the calculations of this model, the probe beam is assumed to be incident nearly normally to the sample surface and also the pump beam is assumed to have sinusoidal variations in its intensity. These assumptions do not exactly fit the geometry of the experimental setup in this thesis, since the probe beam is incident significantly off the normal of the surface. Also the pump beam used to produce the thermal bump is chopped, which produces square waves /train of pulses instead of sinusoidal waves. Hence some appropriate modifications in the model would need to be made to match them with the geometry of the set-up in this thesis.

At this point, no suitable theory exists for the interpretation of the STL data from polymer samples, so the emphasis in this thesis is mainly on the qualitative analysis of the experimental results. The extension of this work, which requires further modifications and development of the model for the quantitative analysis of these results, is left for future researchers.

The summary of the factors affecting the STL signal.

Factors affecting the STL signal	When this factor increases, the STL signal……..
Pump beam Laser Intensity	Increases linearly in the linear regime of the intensity.
Optical Absorptivity	Increases linearly in the linear regime of optical absorptivity.
Thermal diffusivity	Is decreased due to flattening and broadening of the thermal bump.
Coefficient of thermal expansion	Increases.
Modulus of elasticity	Amplitude decreases but the STL signal phase increases.
Pump beam chopping frequency	Decreases if the only factor involved is the amount of energy absorbed.

Chapter 3: APPARATUS

The apparatus used for the experiments done in this thesis was acquired and assembled by previous workers. A schematic representation of the experimental set-up is shown in Fig 3.1 below.
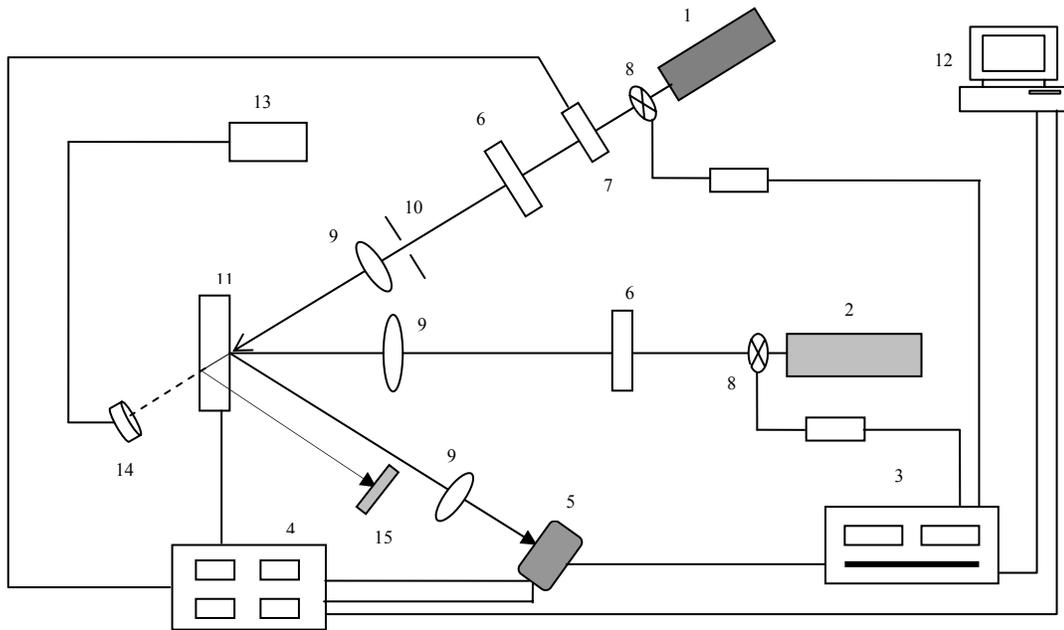

Fig. 3.1 Schematic of the experimental set up for the STL measurements.

1- <u>Probe Beam Laser Source</u> Newport Model ULM 1145 series

The probe beam is produced by a He-Ne class IIIb laser having wavelength of 633nm and a maximum power up to 35 mW and ranges from 0.5 to 25.0 mW with an in-line attenuator. The beam diameter is 0.48 – 0.81 mm. It is focused to approximately 100 μm on the sample.

2- <u>Pump Beam Laser Source</u>   Millennium II Diode-pumped, CW Visible Laser

Its power range is 0.2 – 2.0 W. It is an all solid state laser having visible CW laser

with power > 2 W and wavelength of 532 nm. It runs off of a standard 110/220

V(ac). It is focused to approximately 50 microns on the sample surface.

3- <u>Lock-in-Amplifier</u> Stanford Research Systems; Model SR830 DSP

The lock-in-amplifier picks up a particular frequency signal that matches with the

frequency of the chopper to provide a reference signal input for the lock-in-

amplifier, and the rest is taken as noise. It is used to monitor both the amplitude

and the phase of the measured signal.

4- <u>Motion Controller</u> Model MM 3000 (Newport)

All the four linear actuators are connected to the motion controller, which controls

the motion of the devices to which they are connected. These are the pinhole

detector, the sample, and the attenuator. It gives a reproducible movement of the

devices connected to it, having accuracy of approximately 0.05 microns.

5- <u>Pinhole Photo Detector</u> Model PD-3000 (Precision Applied Science)

The photodetector is a high performance Silicon detector. It can detect fast light

signals from 190 nm to 1700 nm. Its risetime is less than 5.00 ns.

A pinhole is attached to its front to allow detection of a small portion of the

reflected probe beam.

6- <u>Beam Steerers</u>

The beam steerer shifts the beam up or down or sideways without tilting it.

7- <u>Attenuator</u> Model M-935-5-OPT (Newport)

The attenuator is used to control the power of the probe beam. It is placed in the path of the probe beam to control its power using a motorized actuator attached to it. The setting of the attenuator was not changed throughout the experiments; that is, the power of the probe was not varied. The beam through the attenuator showed good stability since its power varied by only one to two milliwatts in a month.

8- <u>Optical Choppers</u>   Model SR 540 (Stanford Research System Inc.)

Optical Choppers are mechanical choppers, each placed in the path of the pump and the probe laser source. These produce a frequency modulated laser beam by chopping a continuous beam for half of the cycle. Both pump and probe choppers chop the beam in the ratio 50:50. The chopping frequency range of these choppers is 4 Hz to 3.7 kHz with a frequency stability of 250 ppm/^{o}C. The frequency drift is less than 2% for the frequency range of 100 Hz to 3.7 kHz. These have a 4-digit frequency display with a resolution and accuracy of 1 Hz.

9- <u>Lenses</u>

The lenses used in this setup are bi-convex. These are used to focus or defocus the

beam on the sample surface. The distance at which these are placed depends on

their focal lengths and on the required beam diameter on the sample.

10- <u>Diaphragm</u>

The diaphragm is an adjustable aperture used to eliminate multiple reflections

from the beam steerer.

11- <u>Sample</u> (G.S Plastic Optics)
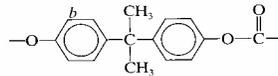
The sample used for analysis is an amorphous bis-phenol A polycarbonate. It is

disc-shaped with a diameter of approximately 25 mm and thickness of 2mm. It is

transparent, having 85-91% transmission in the visible spectrum with the sample

thickness of 3.174 mm.

12- <u>Computer</u> DELL XPS P120c

The computer is a Windows-based machine used to acquire and save data in files

for further analysis.

13- <u>Optical Power Meter</u> Model 1815-C (Newport)

The power meter measures power in the range from nano- to kilowatts.

In this setup it is used to measure the power of the probe beam, incident, reflected, or the transmitted by placing the attached detector (883-SL OD3) in the beam path.

14- <u>Power Detector</u> Model # 883-SL OD3 (Newport)

The power detector is mentioned under the power meter heading (13).

15- <u>Beam Blocker</u>

The beam blocker is used to block the probe beam reflected from the back surface of the sample.

16- <u>Linear Actuator</u>   Model # 850G with travel limits range of 0.8 – 50 mm.

This linear actuator (not shown in the schematic) is connected to the attenuator placed in front of the probe beam laser and controls the power of the beam. It is accurate up to 0.05 μm. The motion of the actuator is controlled by the motion controller channel 4.

17- <u>Linear Actuators</u> Model # 850F (not shown in the schematic)

Two of these are connected to a pinhole detector to move the detector along x and y-axes using motion controller channels 1 & 2. Another actuator is connected to the sample for motion along x-axis and is moved using motion controller channel 3. For motion along the y-axis, a screw gauge is connected and is operated manually. It has an accuracy of 0.05 μm.

18- <u>Non-contact IR thermometer</u> Raytek, Raynger ST 20 x B (not shown in the schematic)

The infrared thermometer is used to measure the surface temperature of a small spot from a distance. It can measure temperature in the range of -30°C to 535°C with an accuracy of ± 1%. The distance to spot ratio is 12:1.

It has a single point laser sighting system that allows it to concentrate all of the laser energy in a single point, showing the center point of the measurement.

19- <u>Filter</u> (not shown in the schematic)

Filter is used to absorb most of the transmitted pump beam to prevent any hazardous effects.

20- <u>Software</u> PTM YC (not shown in the schematic)

PTM YC software package uses Visual Basic 6.0. it was written by Andrew Zhao and then modified by Dr. Thomsen. It can be used to control the lock-in-amplifier, but usually it is used to acquire data by connecting it to the lock-in-amplifier.

21- <u>CCD Camera</u> Model # 250677 (COHU) 6400 Series (not shown in the schematic)

CCD camera is a Charge Conversion Device, which converts light signals to electrical signals. It helps align the probe and the pump beam on a sample spot.

Chapter 4: EXPERIMENTAL PROCEDURE

A schematic of the experimental setup was shown in Fig. 3.1. The entire setup was enclosed in plexiglass to provide a controlled environment. It kept dust out as that could greatly affect the level of noise in the experiment. The enclosure was covered with thick dark cloth to keep any stray radiation from entering and also to protect the user's eyes from the hazardous effects of the laser light.

The pump beam laser source (Chapter 3) was set at 1.0 W for all runs reported here; the beam was projected perpendicular to the surface at a specified spot on the sample. The probe beam laser source (Chapter 3) was set to give approximately 10 mW by using an attenuator. This beam was projected on the sample at an off-normal angle. The pump and the probe beams were aligned to coincide on the same sample spot using beam steerers placed in their paths. The alignment was checked using a CCD camera connected to a monitor outside the enclosure. Inaccurate alignment may affect the stability of the output signal and the phase values.

To optimize the position of the detector, the pump beam was shuttered and the probe beam was chopped. The signal for the lock-in-amplifier came from the detector, and the reference frequency was supplied by the probe beam chopper. The detector position was adjusted using motion controller to obtain an optimized signal, ensuring the detector sits near the peak of the reflected probe beam. Whenever the lock-in-amplifier showed overload, it was set for higher current values till it went no further. In this situation when

it still showed overload, values on either side of the overload for both x and y position on the motion controller were taken, and then average of these values was taken, which was considered to be where the maxima lay.

An alternative method to optimize was to un-shutter the pump beam with the probe chopper turned off and the pump chopper connected to the lock-in-amplifier. This seemed more reliable, but the sample could not be exposed to the pump beam for longer than a few minutes because of the time dependent nature of the signal. So usually the signal was optimized using the first method, which provided an approximate optimized detector position, with the pump beam shuttered. The position was then rechecked with the pump beam unshuttered.

The probe beam chopper was turned off and the pump beam chopper turned on. Now this chopper becomes the reference frequency for the lock-in-amplifier. Its frequency was first set at 67 Hz. This frequency was taken as a reference because it gave strong and stable signal values. The temperature of the spot and the power of the incident, reflected and the transmitted probe beams were recorded. These quantities were also noted at the end of the experiment in order to check for any appreciable variation in their values.

The lock-in-amplifier's time constant was set to one second, and the computer acquired data once per second. An actual irradiation time of 5 minutes was used. The pump beam was unshuttered. The modulated pump beam then reached the sample surface and heated it. A localized deformation, i.e. a thermal bump, was produced, which flexed with the

same frequency as that of the chopped pump beam. The incident probe beam, which

covered the entire pump beam spot, was reflected from the fluctuating thermal bump. An

oscillating diffraction pattern in the reflected probe beam, having the same frequency as

that of the thermal bump, was formed and its maximum intensity signal entered the

pinhole detector, which sent the signal to the lock-in-amplifier. The lock-in-amplifier

amplified the AC part of the signal whose frequency matched with that of the reference

frequency, i.e. the pump beam chopping frequency, and the rest was filtered out. The

phase shift between the input (chopped pump beam) and the output (reflected probe beam

with diffraction pattern embedded in it) and the intensity of the signal were measured by

the lock-in-amplifier. The lock-in-amplifier then sent the data to the computer where a

software package PTM YC using visual basic 6.0 (Microsoft Windows) was used for data

acquisition. The data were displayed in the form of plots (signal amplitude versus time

and phase versus time) and stored into files for further analysis.

One day before the frequency dependent runs on the chosen spot, time decay runs were

done (by Nandita Prasad), a total of 4 hrs. in steps of two 1.5 hrs. and one 1 hr. runs. This

was done to make sure that the signal did not decay appreciably during each five minutes

run.

The frequency dependent runs constituted 5 minute runs at frequencies starting from

37 Hz to 418 Hz in steps of 10, 20, 30, and 40 Hz. At low frequencies more data were

collected because the signal varied rapidly at low frequencies as compared to at high

frequencies. A 5 minute run at 67 Hz before and after each frequency run was performed

in order to correct for the remaining time dependence in the signal. The pump beam was shuttered after each run, and the chopper was then set for a new frequency. The average of the data for each run was taken as one data point for that particular frequency.

At the end of the experiment, before shutting down, care was taken to reset the motion controller to 00.00 setting; otherwise its origin would shift to the value at which it was turned off.

Chapter 5: RESULTS AND DISCUSSION

A specific sample spot that shows trends fairly common throughout the experiments performed is chosen for discussion.

It has already been mentioned in Chapter 3 that at every new sample spot, the time dependence of the STL signal must be diminished in order to study its frequency dependence. Thus frequency dependent studies were preceded by several hours of exposure of the sample spot to a 67 Hz chopped beam while the amplitude decay was observed. Exponential time dependence had been observed, only for polymer samples, by previous workers in the lab. No exponential amplitude decay has been observed by previous workers while working on inorganic samples.

An important aspect to note here was that even though the decay was carried out at a chopping frequency of 67 Hz– that is, the sample spot was conditioned for 67 Hz– the time dependence also similarly disappeared for other frequencies too. So the sample spot was also conditioned for all the frequencies used in the experiments. An example is shown in Fig. 5.1. The dotted lines mark points at which the experiment was interrupted to save data. The reduction of the time-dependence of the signal was found to be a permanent and irreversible phenomenon because signal values were observed to resume at the same value where they left off in the previous run. Occasionally a slight variation was observed when the sample was left alone for an extended time (several days) before measurements were made on the same spot. The signal was occasionally somewhat

higher than where it left off previously, but it was never as high as the original value.

Hence frequency dependence runs were not significantly affected by taking the data one

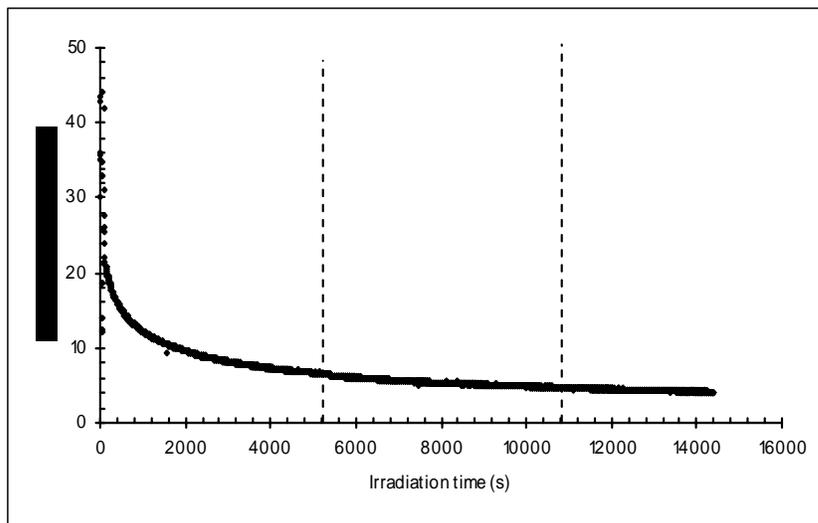or two days following the conditioning of the sample spot.

Fig. 5.1 STL signal (amplitude) versus pump beam irradiation time, during conditioning
(by Nandita Prasad).

Analysis of the data obtained here is based on the STL theory discussed in Chapter 2, and

effort is made to characterize various features of the data to obtain information on the

optical, thermal, and mechanical properties of the polymer sample.

Previous workers in the lab have found that there is not always a linear relationship

between the photothermal signal and the pump beam intensity for all intensity values.

The work here is done by using the intensity value that lies in the linear regime.

Therefore, it is justified here to say that the photothermal signal varies linearly with the

intensity. As discussed in Chapter 2, this implies the STL signal amplitude is also linear in the optical absorptivity.

STL Signal Amplitude versus the Pump Beam Chopping Frequency

Fig. 5.2 shows the relationship between the STL signal (amplitude) and the pump beam chopping frequency. The amplitude rises with the frequency, reaching a maximum at approximately 67 Hz, and then it decreases with increasing frequency.
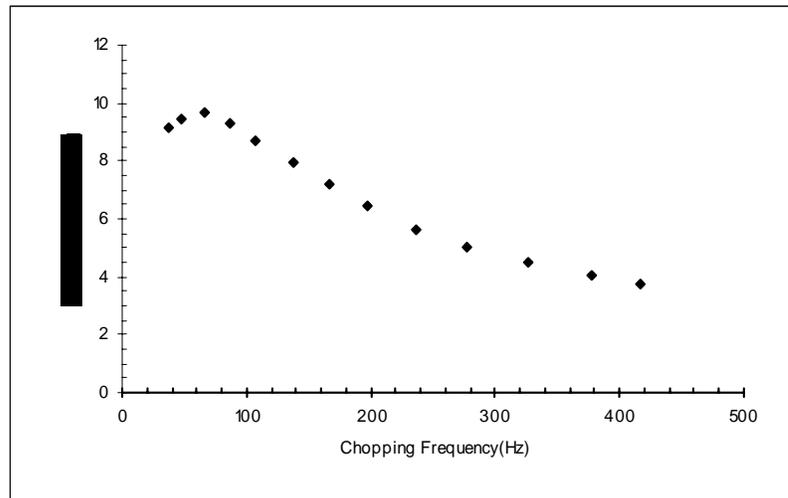

Fig. 5.2 STL signal (amplitude) versus pump beam chopping frequency.

Fig. 5.3 shows the plot for the signal amplitude at 67 Hz versus the number of times the data are acquired at this frequency. Each data point represents the signal amplitude value either before or after the runs at frequency values shown in Fig. 5.2. This curve represents the time-dependence of the signal amplitude. As already mentioned, each sample spot was exposed to the modulated pump laser beam for four hours prior to these

measurements, in order to diminish time-dependence. The graph presented here shows a

little time-dependence still present even after this conditioning of the sample spot, but at

some other spots this time-dependence is completely removed. To eliminate the effect of

this time-dependence, the signal amplitude versus frequency curve is normalized,

dividing the signal amplitude at any given frequency by the average of the amplitude at

67 Hz taken immediately before and immediately after the data taken at that particular

frequency. These normalized plots then can be used to compare the results of each

sample spot. Fig. 5.4 below represents the curve with 67 Hz normalization.
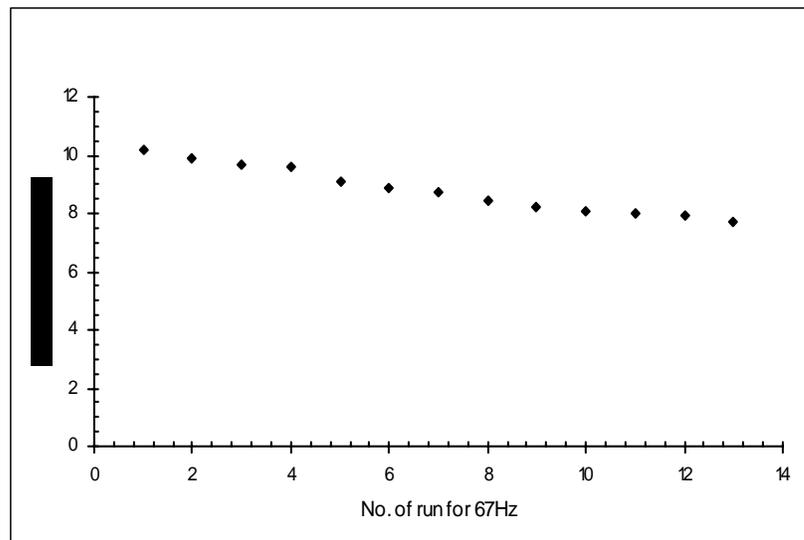

Fig. 5.3 STL signal (amplitude) versus number of run for 67 Hz.

Theories and models[66, 77, 78] developed so far explain the decay part of the curve very

well, but there is not a convincing explanation for the peak at a particular frequency.

According to the thermal wave theory, the thermal diffusion length of the waves

decreases with increasing frequency (since $\mu \propto f^{-1/2}$); that is, the thermal waves decay

more rapidly at higher frequencies than at lower frequencies. If there is no diffusion, then

the temperature profile is equal to the beam profile. Thermal diffusion broadens the

profile, reducing the curvature. Thermal diffusion has less effect on curvature at higher

frequencies than at lower frequencies; therefore, thermal diffusion tends to decrease the

curvature more at low frequencies. The curvature of the thermal bump is linearly related

to the size of the peak formed in the *diffraction* pattern of the reflected probe beam.

Therefore, the STL signal is decreased by thermal diffusion more at lower frequencies
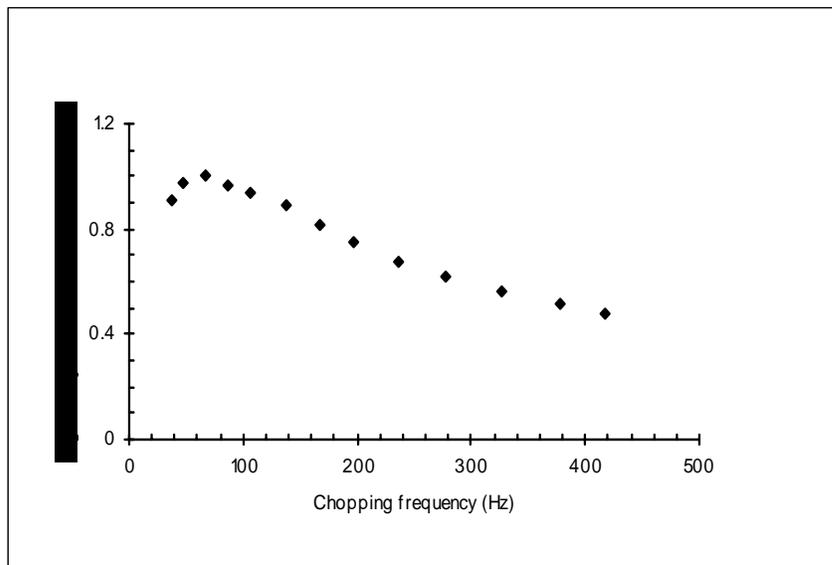
than at higher frequencies.

Fig. 5.4 STL signal (amplitude) with 67 Hz normalization versus the pump beam

chopping frequency.

The observed peak in the amplitude versus the chopping frequency plot deviates from the

thin film[94] behavior, suggesting that some different phenomenon is occurring in the bulk

sample as compared to the thin films. This argument will have more validity if

comparison is made with the thin film and the bulk sample of the same material and using an extended frequency range, because there is a possibility that the peak might have existed at a lower frequency for thin films than were studied.

The longer the pump beam is incident on the sample, the greater the energy absorbed. When this energy is transformed into thermal energy, it causes localized thermal expansion. The size of the mechanical bump depends on the thermal expansion coefficient, thermal diffusivity, and the elasticity of the sample spot. At a given frequency, the time for which the sample is exposed to the pump beam is equal to the time for which the beam is chopped. During the time for which the pump beam is chopped, the absorbed energy diffuses from the sample spot and into the surrounding material. The diffusion rate depends on the thermal diffusivity of the sample spot. The thermal bump, developed in the first half cycle of the modulated pump beam, may or may not relax completely during the chopped portion of the pump beam. If the thermal bump relaxes completely, then there may or may not be complete mechanical relaxation of the mechanical bump. But if there is not a complete thermal relaxation, then most probably mechanical relaxation is also incomplete. These possibilities are dependent on the thermal and mechanical properties, mainly the thermal diffusivity and either the elasticity or the relaxation time τ, of the sample spot. These properties may vary from one spot to the other, but are assumed to be constant at one spot. A change in temperature may cause variation in these properties, but the change in temperature is calculated to be not more than one or two degrees Celsius, not enough to produce a significant change in these properties[95].
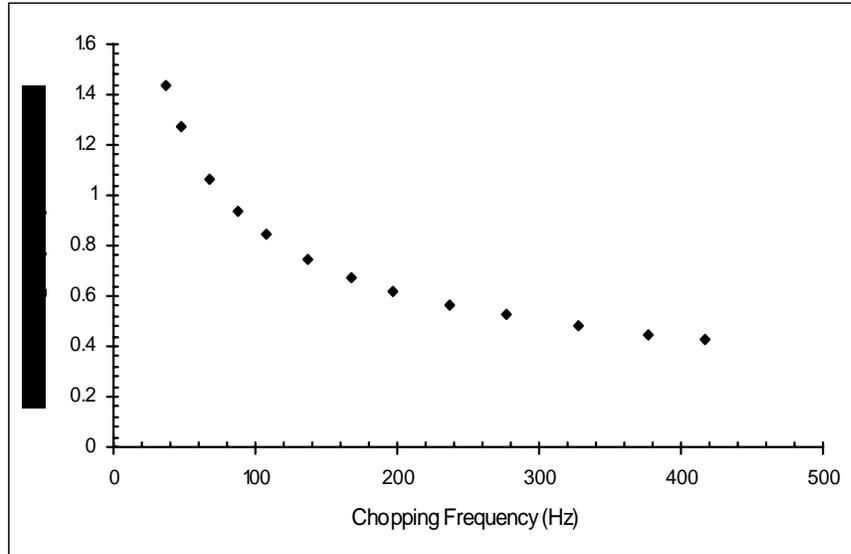
Fig 5.5. Ratio of thermal diffusion length to pump beam radius versus chopping frequency.

It is suggested that the thermal bump relaxes completely during the time the pump beam is chopped if the thermal diffusion length, μ, is much greater than the pump beam radius, R_o. The graph for μ / R_o versus frequency is shown in the Fig. 5.5. The thermal diffusion length is calculated by using Eq. (2.3). The thermal diffusivity of the polycarbonate sample, calculated using Eq. (2.5), is found to be 1.5 x 10^{-7} m^2/s, with k=0.21 W/m·K, ρ= 1.2E6 g/m^3, and c= 1.17 J/gK [87]. This value of thermal diffusivity is used to calculate the thermal diffusion length (Eq. 2.3) at each chopping frequency, which is then divided by the radius of the pump beam (R_o= 2.5 x 10^{-5} m). The ratio is then plotted versus the chopping frequency (Fig. 5.5). The plot suggests that the thermal bump does not relax completely and the amount of thermal relaxation decreases with frequency. This is only an approximate result because the ratio, μ / R_o, is calculated by taking average values of thermal conductivity, the density, and the specific heat (these values typically vary from

44

spot to spot in a polymer). Hence all possibilities for both thermal and mechanical relaxation need consideration.

Suppose the bump does not relax completely. Its height keeps increasing until it reaches saturation after a while; then a steady state condition is reached. The height of the bump increases initially because of the low rate of thermal diffusion due to the smaller temperature difference between the sample spot and its surroundings. But with time the temperature difference builds up, increasing the rate of thermal diffusion, and eventually a point is reached at which the amount of thermal energy flowing out from the sample spot equals the amount of energy deposited. At this state there is no further rise in the bump height; that is, saturation is reached and the condition is called the steady state condition. The situation may look qualitatively like the curve shown in Fig. 5.6(a).

On the other hand, Fig. 5.6(b) represents a complete thermal and mechanical relaxation during each cycle and thus a steady state is reached instantaneously. The only difference between the two cases is the height of the bump. By the time steady state is reached for both cases, the fluctuations are similar. Since the STL signal is the *variation* in the bump, there seems to be no significant difference in the extraction of the information in either the complete or the incomplete thermal and mechanical relaxation. To extract information about whether the thermal and mechanical relaxation is complete would require additional experiments designed specifically to detect the absolute bump height. There would be, for instance, a difference in the DC STL signal, but it is not clear if it would be large enough to detect.
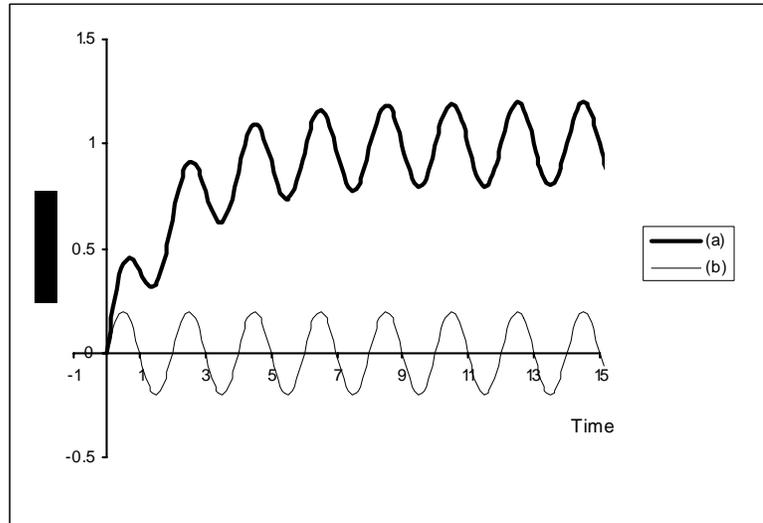
Fig. 5.6(a) Schematic representation of the bump height versus time with incomplete

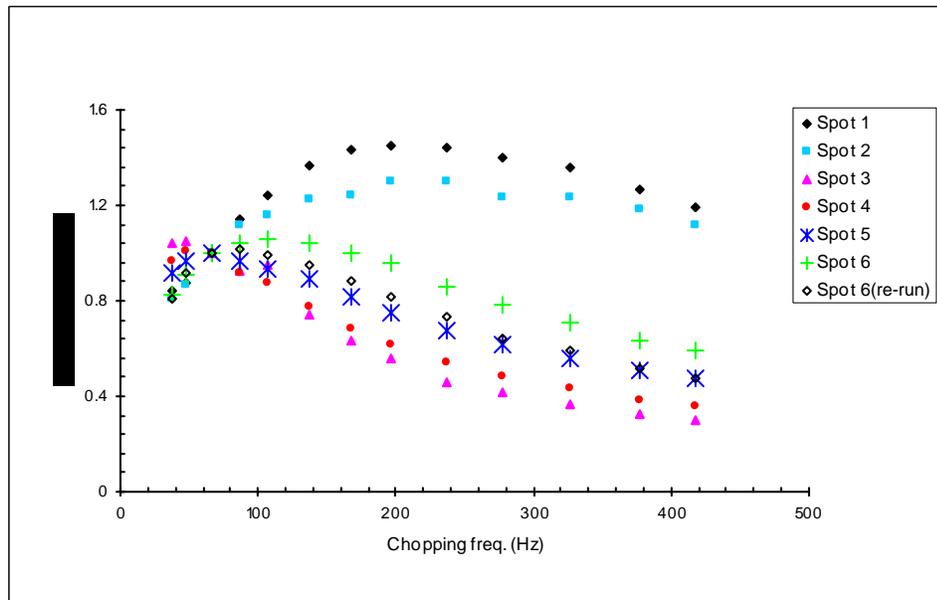relaxation during each cycle and (b) with complete relaxation. (units are arbitrary)

Fig 5.7- STL signal (amplitude) with 67 Hz normalization versus pump beam chopping

frequency curves for different sample spots.

By looking at the signal amplitude versus frequency curves at various sample spots, it is observed that the peak at different sample spots occurs at different frequencies, shown in Fig. 5.7.

The spot 6(re-run) is the re-run on spot 6 without shuttering the pump beam in between the five minute run at each frequency. The data do not show any significant change in the trend. Hence, once the spot is conditioned it stays conditioned.
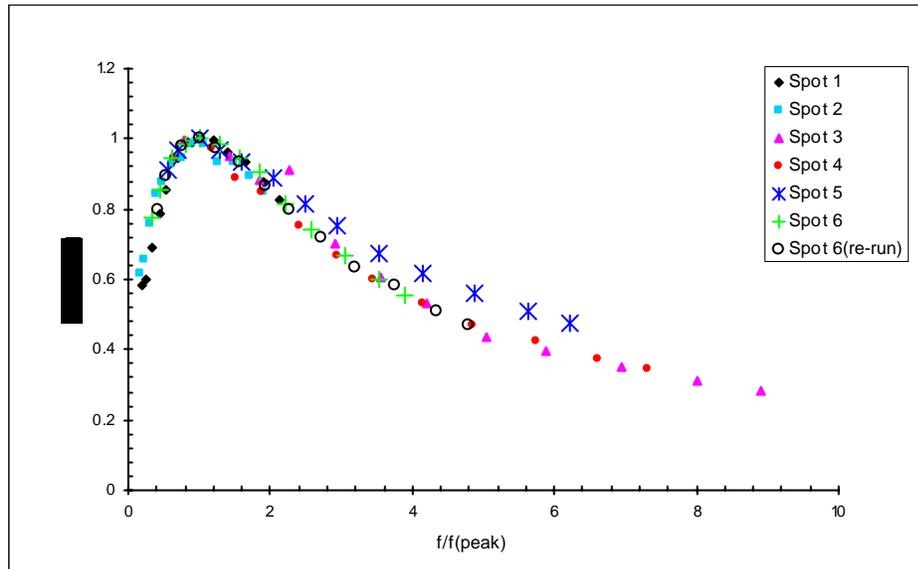

Fig. 5.8 Normalized STL signal (amplitude) R/R(peak)* versus normalized chopping frequency f/f(peak) curves for different sample spots.

To observe similarities and differences, the signal amplitude and frequency are normalized, dividing them by their respective values where the peak occurred for a specific spot. These curves are shown in Fig. 5.8.

The nearly complete overlapping of all the curves showing a general trend suggests a common underlying mechanism governing the behavior at each sample spot and represented by a single mathematical relation. The shift in the peaks at different sample spots suggests variation in the optical, thermal, and/or mechanical properties that enter into the underlying mathematical relation.

Phase Lag versus Pump Beam Chopping Frequency

Fig. 5.9 shows the curve for the phase versus the pump beam's chopping frequency. There is a gradual increase in the phase lag with the chopping frequency.
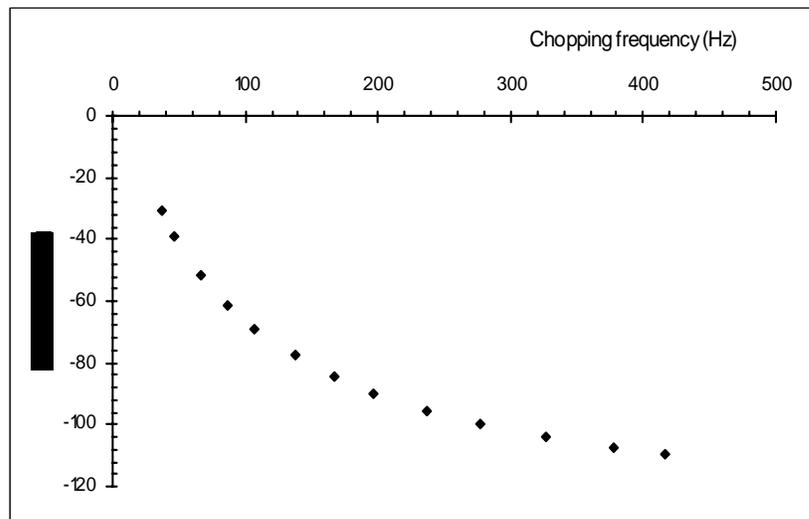

Fig. 5.9 Phase lag versus pump beam chopping frequency.

The trend in Fig. 5.9 shows a smaller phase lag at lower frequencies than at higher frequencies. This phase lag is the difference in the phase of the input signal, i.e. the chopped pump beam, and the output signal (reflected probe beam). Phase lag tells us about the delay in the sample spot responding to a stimulus.
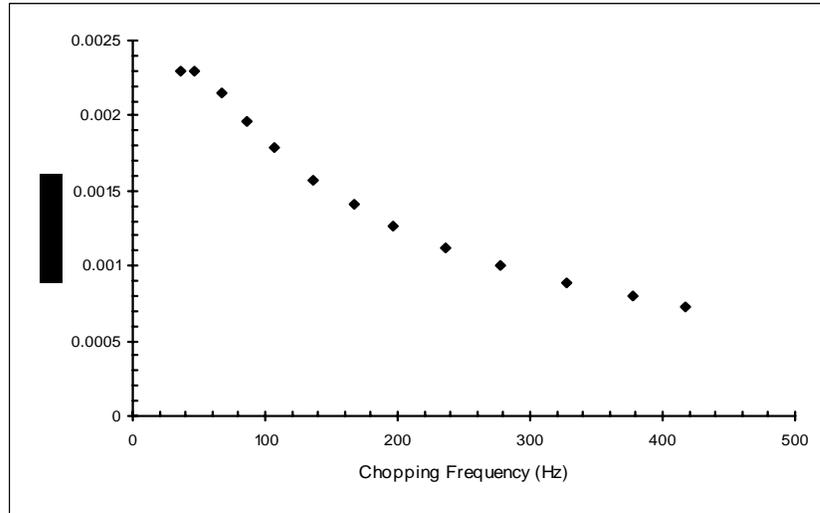

Fig. 5.10 Time lag versus pump beam chopping frequency.

Fig. 5.10 shows the relation between the time lag and the pump beam chopping frequency. The values for the time lag, T_L, are calculated by using Eq. (2.6) and the data from Fig 5.9. The curve shows a regular decrease in the time lag with the chopping frequency.

As the pump beam is turned on, heat initially gets absorbed and then diffuses out from the center. The absorbed heat causes thermal expansion, forming a bump on the surface of the sample spot. How quickly the spot responds to form the bump depends mainly on its elasticity. A perfectly elastic material will respond instantaneously to a modulated

mechanical stress, but any delay in the response is a property of a viscoelastic material. Here the stress-causing source is the modulated laser beam. Initially, the optical energy-producing localized thermal stresses cause expansion in the sample spot. But the response time for optical absorption is very small; hence the only significant contribution to the phase lag is due to the elasticity of the sample spot.

At lower frequencies the pump beam is incident on the sample for a longer period of time than at higher frequencies, causing stress for a longer time. This reduces the elastic modulus more at lower frequencies than at higher ones. Since mechanical relaxation time is the ratio of viscosity of the sample to its elastic modulus, the relaxation time therefore decreases with frequency, which is observed in Fig. 5.10.

Another phenomenon that may be responsible for this decrease in the time lag is stress relaxation. By analogy, if a rubber band is stretched several times, then after some time it requires less stress to produce the same strain, i.e. its modulus decreases with time. This phenomenon is called stress relaxation. This situation may have occurred in the case of repeated flexing of the bump at the surface of the sample spot, thus reducing its modulus and increasing its viscous behavior (becoming softer). This softening can also be due to the size of the bump. At low chopping frequencies more energy gets absorbed, producing a bigger bump, than at higher frequencies, softening the sample spot more at lower frequencies. This may tend to increase the time lag more at lower frequencies than at higher ones (Fig 5.10).

Fig. 5.11(a) shows the variation in the phase with the pump beam chopping frequency for a number of sample spots.
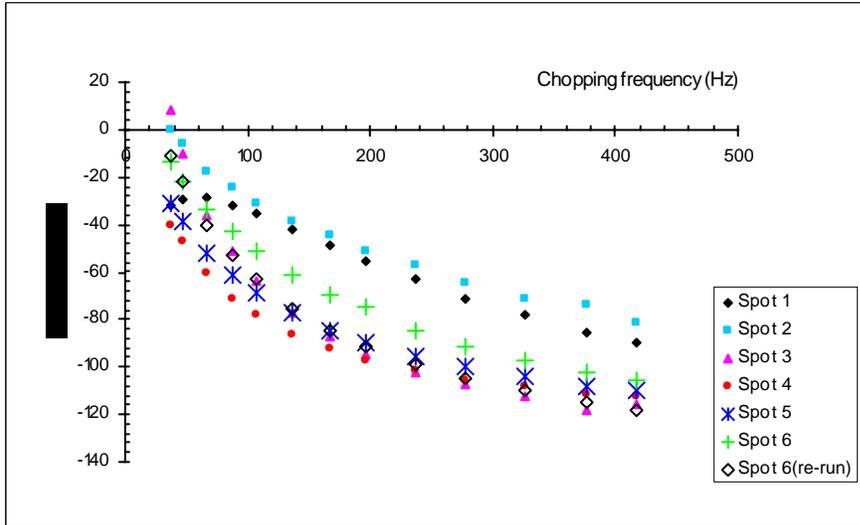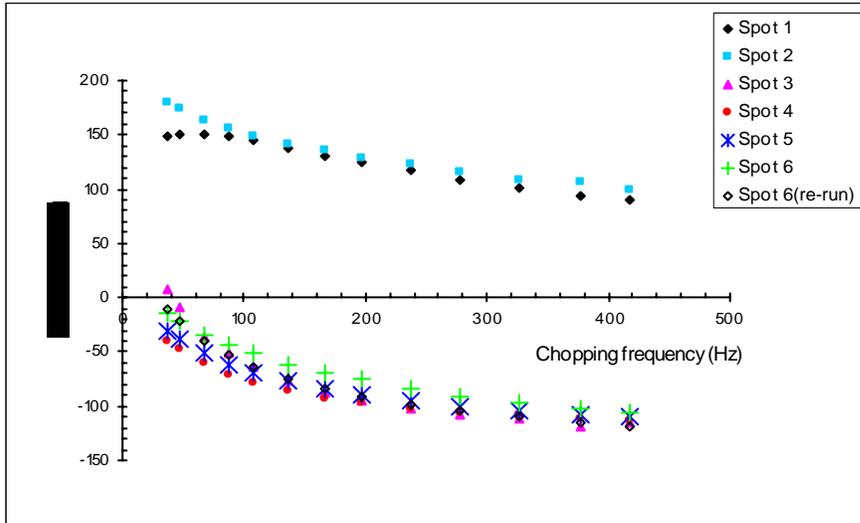

Fig. 5.11(a) Phase lag versus chopping frequency curves for different sample spots. (b) Same with data from spots 1 and 2 shifted.

Most of the curves overlap, suggesting some common physical phenomenon occurring at every spot. Since these plots are not normalized, it may be that a single mathematical

51

relation can approximately describe these curves without any variation in its parameters, that is, no variation from one spot to the other in the properties that cause the phase lag.

Two curves lying in the positive phase region seem to be the outliers, but if 180° is subtracted from the phase values of these curves, then they overlap with the rest of the curves shown in Fig. 5.11(b). In order to justify this, a hypothesis[95] is made according to which the pinhole detector might be centered on the first minimum instead of the central maximum of the diffraction pattern. This is possible because the detector is repositioned every time between runs at different spots so that it sits at a local maximum in the STL amplitude. However, both a maximum and a minimum in the diffraction pattern will produce a local maximum in the STL amplitude. If the detector had been sitting at a diffraction minimum, then it is justified to subtract 180° from the actual phase.

All the spots in Fig 5.11(b) show the same behavior as the spot shown in Fig 5.9. Therefore, the time lag behavior for these spots is the same as the time lag behavior for the first spot discussed earlier. The qualitative understanding of the time lag and the phase lag applies equally to the entire set of spots.

As the normalized signal amplitude versus the normalized frequency plots have proven to be useful in the interpretation of the amplitude data obtained at different spots, it may be interesting to examine the normalized plots for the phase as well.
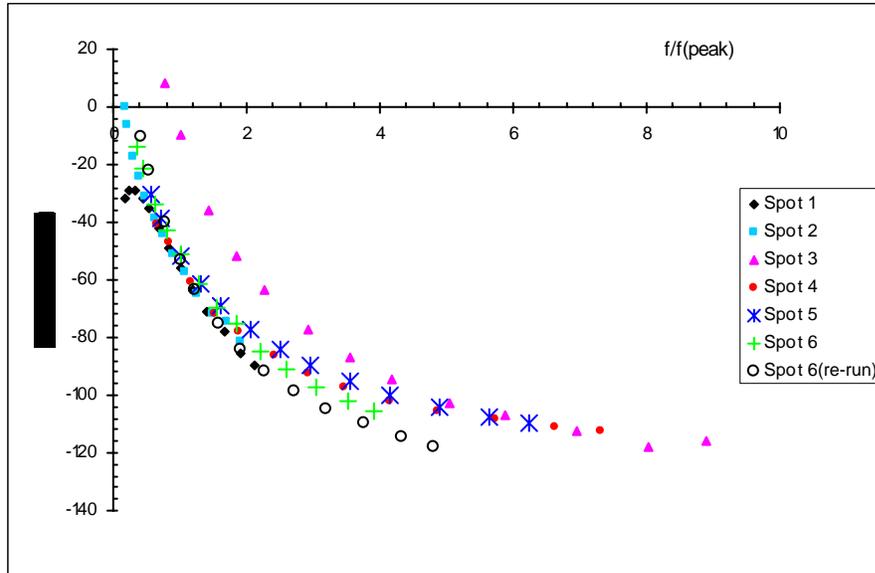
Fig. 5.12 Phase lag versus normalized pump beam chopping frequency.

Figure 5.12 shows the combined curves for the phase versus the normalized frequency where the same frequency normalization factors have been used that were used in Fig 5.8. By comparing the two figures, Fig 5.11(b) and Fig 5.12, we see some improvement in the collapse of the data onto a single curve, which suggests some variation in the properties, causing the phase lag, of the polymer from one spot to the other.

The Fig 5.13 represents the normalized signal amplitude versus the normalized frequency curves with an outlier spot added in. This was the only spot (neglecting defects discussed in the next section) observed that did not fit the previously described trends.
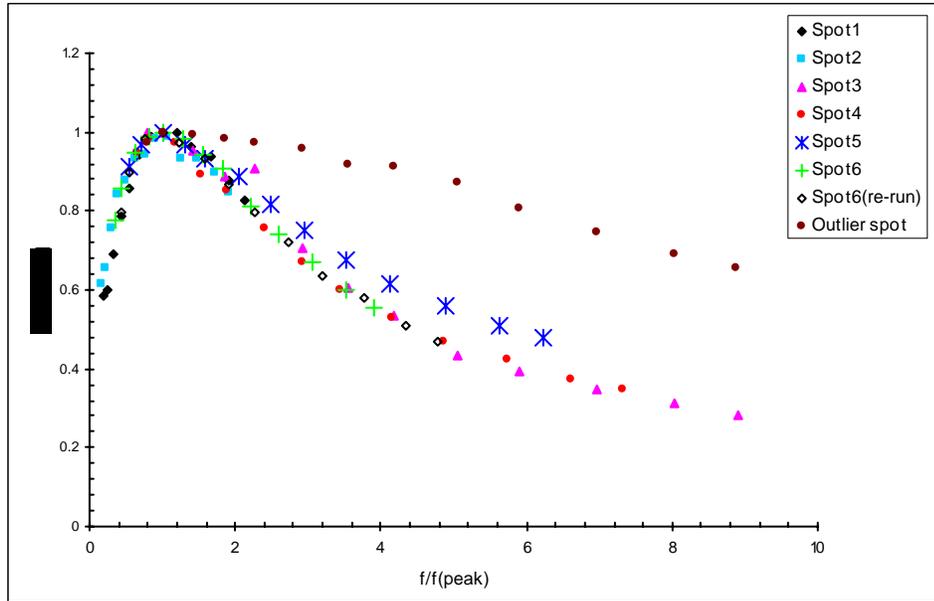
Fig. 5.13 Normalized STL signal (amplitude) R/R (peak) versus normalized chopping frequency f/f (peak) curves for different sample spots with an outlier spot included.
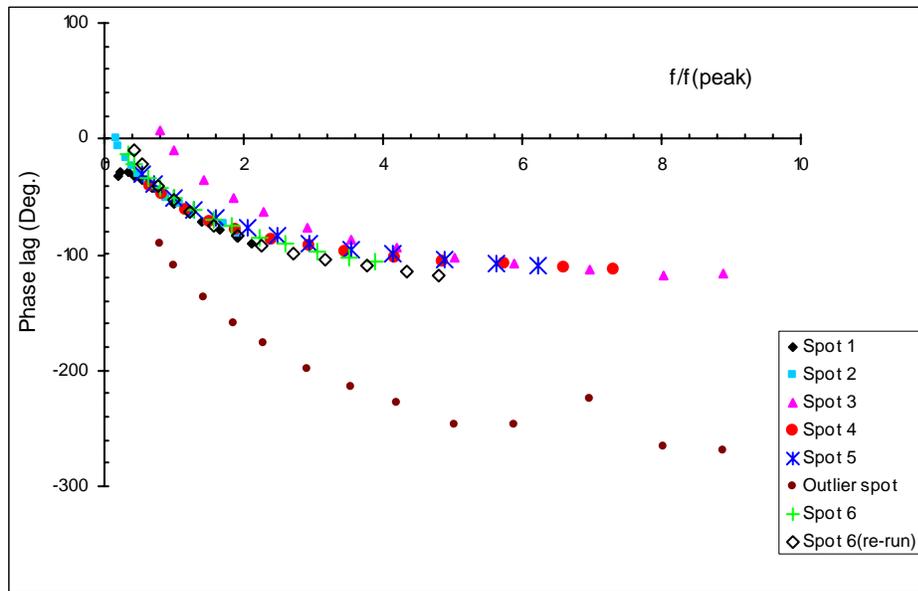

Fig. 5.14 Phase lag versus normalized chopping frequency with an outlier spot included.

54

A number of normalization procedures were applied to in an attempt to make the outlier spot curves for both the signal amplitude and the phase to collapse with their respective curves, but no such collapse was obtained. One important aspect to note here is that both the curves for the outlier spot showed similar trends as the rest of the spots when compared without normalizing, but they did not overlap with the rest of the curves when normalized. This lack of overlap suggests some different mechanism is involved, which is not known at this stage.

Complications and Limitations

During the runs at a few spots, a different phenomenon occurred that completely destroyed the spot for further analysis. The spot seemed to have a hole drilled in it. This might have been due to ablation, which is caused by breaking of chemical bonds due to absorption of energy equal to or greater than the dissociation energy. The result is the production of a large number of small, volatile fragments that are then evaporated as the pressure builds up due to these numerous fragments in a small volume. There could be a localized viscous flow of the material, but it did not seem to be the case since no bumps around the holes were seen when viewed through a magnifying glass. This phenomenon occurred on new sample spots as well as on the old ones (where data had already been acquired). It was observed that the defects occurred after the pump beam was unshuttered.

The reason for this phenomenon is not yet clear. It may be due to degradation of the sample with time and exposure to radiation, but the defects also occurred at new spots that were not exposed to the laser beam. Other possibilities are contamination in the surrounding air, melting of the wax on the front surface that was used to hold the sample position, and/or occurrence of some chemical changes in the sample itself.

When the sample was viewed closely, one of the defects was seen to occur on the back side of the sample, eliminating the factor of melting of the wax on the front surface to

form a thin film on it. Hence, the most likely cause is some chemical change in the material itself.

The generation of these defects limited the number of spots from which useful data could be acquired. The sample became completely unusable as further exposure to the pump beam always caused defects before sufficient data could be acquired for analysis. It is thus suggested that additional experiments should be done on thin films with polycarbonate as a coating to observe if similar defects also occur in thin films, since such defects have not been observed in thin films in the past. These observations should also be made on different bulk samples and their respective thin films with special emphasis on polymers, to find out if the phenomenon is specific to bulk samples.

A few images of the defects are shown on the next page. These are a series of images of a single defect. Images of figures (c) and (d) are magnified four times more than the images of figures (a) and (b). The defect is approximately 1 mm long and 0.5 mm across.

(a)

0   0.1mm

(b)

0   0.1mm
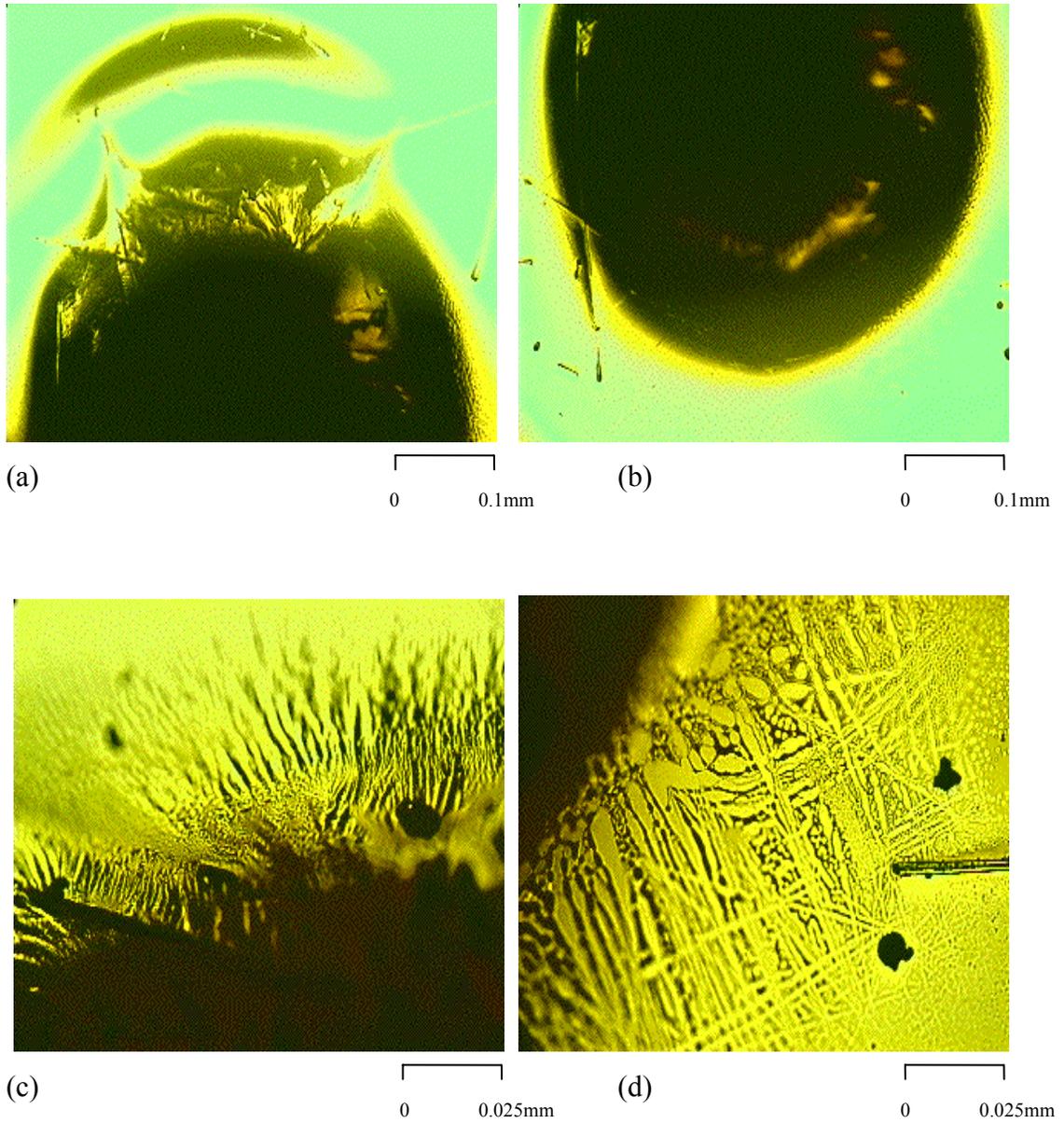
(c)

0   0.025mm

(d)

0   0.025mm

Fig. 5.15 Images of a defect using LEICA DMRB/E Light Transmission Microscope.
(a) Top part of the defect. (b) Bottom of the defect. (c) Edge of the same defect, further
magnified four times. (d) Another edge of the same defect also magnified four times.

Chapter 6: CONCLUSIONS

The Surface Thermal Lensing technique was used to study the phenomena occurring in a bulk polycarbonate sample and to study the effects of its properties on these phenomena. The results were discussed only qualitatively since no model or theory has yet been developed to connect sample properties to STL signals. The thermal and mechanical properties, such as the thermal expansion coefficient, the thermal diffusivity, and the elasticity of the sample, determine the size of the thermal and mechanical bump.

A general trend for both the signal amplitude and the phase versus frequency strongly suggest a common underlying mechanism governing the behavior at each spot. But variation in the position of the peak in the signal amplitude versus frequency curves at each spot suggests variation in the optical and thermo-mechanical properties. But as seen in the phase lag versus frequency curves, properties such as elasticity do not significantly vary from spot to spot.

It is interesting to see in Figs. 5.7 and 5.11 how well the signal amplitude curves as well as the phase curves collapse with similar scaling procedures (normalization). Each of these collapsed curves can be represented by a single mathematical relation. Once an appropriate mathematical function is developed especially for the signal amplitude curve, relating the peak height and its location on the frequency dependent curves with the pump beam chopping frequency, it will then be possible to extract information about the variation in the properties as well as their numerical values at each spot.

One phenomenon not yet understood was whether thermal and mechanical relaxations were complete during the chopped part of the modulated pump beam. It was argued here qualitatively that complete or incomplete thermal and mechanical relaxation was unlikely to have any significant effect on the extraction of information about the sample.

The observed deviation of the bulk behavior from the thin film may suggest some different phenomenon occurring in the bulk as compared to thin films. Hence, further research is required on the bulk polymer samples, especially polycarbonate. The initial time dependence was observed in polymer films by previous researchers and has not yet been understood; therefore, work must be done to understand this time dependence. It might have some impact on the frequency dependent results and could facilitate understanding of these results.

There is a strong need to understand the cause of the defects produced on the sample, which greatly limited the number of the sample spots available for data acquisition. In addition to any changes for future experiments in this regard, visual surface inspection before and after each experiment should be included. This would probably help understand any structural and chemical changes on the surface of the sample.

To explain the existence of the peak in the signal amplitude versus frequency curves, an effort must be made in developing an extensive and a detailed model. Furthermore, similar experiments must be performed on thin films with the coating of the same polycarbonate used here as a bulk sample. An extended frequency range may be used to

eliminate the possibility of occurrence of the peak at a lower frequency for the thin film. These experiments must also be performed on other polymers, taking their bulk as well as their respective thin film samples.

The outstanding collapse of all the data to a single curve after normalizing highlights the importance of developing a new model, which will help us to better understand the similarities and differences between the sample spots.

REFERENCES

[1] A.Rosencwaig; *Photoacoustics & photoacoustic spectroscopy*, (John Wiley & Sons, NY, 1980).

[2] O. Pessoa, Jr., C.L. Cesar, N.A. Patel, H. Vargas, C.C. Ghizoni, and L.C.M. Miranda, J. Appl. Phys. **59**, 1316 (1986).

[3] A. M. Mansanares, M.L. Baesso, E.C. da Silva, F.C.G. Gandra, H. Vargas, and L.C.M. Miranda, Phys. Rev. B 40, 7912 (1989).

[4] M.L. Baesso, A. M. Mansanares, E.C. da Silva, H. Vargas, and L.C.M. Miranda, Phys. Rev. B 40, 1880 (1989).

[5] D.C. Fork and S.K. Herbert, Photochem. Photobiol. **57**, 207 (1993).

[6] W.J. Silva, L.M. Priolli, A.C.N. Magalhaes, A.C. Pereira, H. Vargas, A.M. Mansanares, N. Cella, L.C.M. Miranda, and Alvarado-Gil, Plant Sci. **104**, 177 (1995).

[7] Yue Han, Joseph S. Rosenshein, Z.L. Wu, Wen Ye, Marshall Thomsen and Qiang Zhao, Opt. Eng. **40(2)**, 303 (Feb. 2001).

[8] A. Lachaine and P. Poulet, Appl. Phys. Lett. **45**, 953 (1984).

[9] A.Torres-Filho, L.F. Perondi and L.C.M. Miranda, J. Appl. Polym. Sci. **35**, 103 (1988).

[10] A. Sánchez-Lavega, A. Salazar, A. Ocariz, L. Pottier, E. Villar, E. Macho, Appl. Phys. A, **65**, 15 (1997).

[11] H. Vargas, L.C.M. Miranda, Rev. of Sci. Inst., **74(1)**, 794 (2003).

[12] D. Fournier, A.C. Boccara, N. Amer and Gerloch, Appl. Phys. Lett. **37**, 519 (1980).

[13]L.R. deFreitas, A.M. Mansanares, and E.C. da Silva, Rev. Sci. Instrum. **74**, 735 (2003).

[14]Achim Eickmeire, Thomas Bahners, Eckhard Schollmeyer, J. Appl. Phys. **70**(10), 5221 (1991).

[15]Marcos Gugliotti, Mauricio S. Baptista, Luis G. Dias, and Mario J. Politi, Appl. Opt. **38**(7), 1213 (1999).

[16]Chuan Hu, Ennis T. Ogawa, and Paul S. Ho, J. Appl. Phys. **86**(11), 6028 (1999).

[17]N. Marquardt, V. John, B.K. Bein, I. Delgadillo, A. Haj-Daoud, j. Gibkes, J. Pelzl, Proc. EPAC 2000, Vienna, Austria, pp. 2275

[18]J. C. Murphy and L. C. Aamodt, eds., *Photoacoustic and Photothermal Phenomena II*, Vol. 62 of the Springer Optical Science Series (Springer, Berlin, 1990).

[19]D. Bićanié, ed., *Photoacoustic and Photothermal Phenomena III*, Vol. 69 of the Springer Optical Science Series (Springer, Berlin, Heidelberg, 1992).

[20]A. Mandelis, ed., *Priciples and Perspectives of Photothermal and Photoacoustic Phenomena*, Vol. 1 Progress in Photothermal and Photoacoustic Science and Technology Series (Elsevier, New York, 1992).

[21]Ennis T. Ogawa, Chuan Hu, and Paul S. Ho, J. Appl. Phys. **86**(11), 6018 (1999).

[22]J. E. de Albuquerque, W. L. B. Melo, and R. M. Faria, Rev. Sci. Instrum. **74**(1), 306 (2003).

[23]M. A. Olmstead, S. E. Kohn and N. M. Amer: Bull. Am. Phys. Soc. **27**, 227 (1982).

[24]J. Opsal, A. Rosencwaig and D. L. Willenburg: Appl. Opt. **22**, 3169 (1983).

[25]Y. Chen, M.S. thesis, Eastern Michigan University, 2000.

[26]S. Bandi, M.S. thesis, Eastern Michigan University, 2002.

[27]E. Welsch and D. Ristau, Appl. Opt. **34**(31), 7239 (1995).

[28]Z. L. Wu, M. Reichling, X. Q. Hu, K. Balasubramanian, and K. H. Guenther, Appl. Opt. **32**, 5660 (1993).

[29]M. Commandre, P. Rolhe, J.-P. Borgongno, and G. Albrand, Proc. SPIE **2253**, 982 (1994).

[30]W. C. Mundy, R. S. Hughes and C. K. Carniliga, NBS. Spec. Publ. **669**, 349 (1982).

[31]J. Abate, A Schmid, M. Guardalben, D. J. Smith, and S. D. Jacobs, NBS. Spec. Publ. **688**, 385 (1983).

[32]W. C. Mundy, J. E. Ermshar, P. Hanson, and R. S. Hughes, NBS. Spec. Publ. **688**, 360 (1983).

[33]A. F. Stewart, A. Rusek, and A. H. Guenther, NIST Spec. Publ. **775**, 245 (1988).

[34]S. Watkins, R. Heimlich, and R. Reis, Jr., Proc. SPIE **1624**, 246 (1991).

[35]Z. L. Wu, Z. X. Fan, M. Reichling, D. Schaefer, and E. Matthias, Proc. SPIE **1642**, 271 (1992).

[36]A. Bodemann, M. Reichling, N. Kaiser, and E. Welsch, Proc. SPIE **2114**, 405 (1993).

[37]E. Welsch and M. Reichling, J. Mod. Opt. **40**, 1455 (1993).

[38]M. Reichling, A. Bodemann, and N. Kaiser, Proc. SPIE **2428**, 307 (1994).

[39]M. Commandre and E. Pelletier, Appl. Opt. **29**, 4276 (1990).

[40]Z. L. Wu, C.Z. Tan, and J. Arndt, Proc. SPIE **1848**, 224 (1993); Radiat. Effects Defect. Solids **137**(1-4), 179 (1995).

[41]E. Matthias, H. Groenbeck, E. Hunger, M. Reichling, E. Welsch and Z.L. Wu, "Photoacoustic and Photothermal investigation of thin films", in *Springer Series in*

Optical Sciences, Vol. 69, pp. 436, Springer-Verlag, Berlin, Heidelberg, New York (1992).

[42]Z. L. Wu, M. Reichling, Z. X. Fan, X. Su, and Z. J. Wang, Proc. SPIE **1441**, 241 (1991).

[43]Z. L. Wu, M. Reichling, Z. X. Fan, X. Su, and Z. J. Wang, Proc. SPIE **1441**, 200 (1991).

[44]E. Matthias and R. W. Dreyfus, "From laser-induced desorption to surface damage," in *Photoacoustic, Photothermal and Photochemical Processes at Surfaces and in Thin Films*, Topics in Current Physics, Vol. 47, P. Hess, Ed., p. 89, Springer-Verlag, Berlin, Heidelberg, New York (1989).

[45]S. Petzoldt, A. P. Elg, J. Reif and E. Matthias, NIST Spec. Publ. **801**, 180 (1990).

[46]K. Ettrich, H. Blaschke, and E. Welsch, Proc. SPIE **2714**, 426 (1996).

[47]Q. Zhao and Z.A. Fan, Proc. SPIE **2714**, 331 (1996).

[48]René Krupka and Z. L. Wu, Proc. SPIE **2864**, 286 (1996) Denver Colorado.

[49]P. A. Temple, "Thin Film absorptance measurements using laser calorimetry", *in Handbook of Optical Constants of Solids*, ed. E.D. Palik, Vol. 1, 135, Academic Press, New York, 1985.

[50]V. Loriette, J.P. Roger, A.C. Boccara, Ph. Gleyzes and J.M. Mackowski, Journal De Physique III **4**, C7-631, 1994.

[51]M. Commandre and P. Roche, Appl. Opt. **35**, 5021 (1996).

[52]Z. L. Wu, M. Thomsen, P. K. Kuo, Yuesheng Lu, Christopher Stolz and Mark Kozlowski, Opt. Eng. **36** (1), 251 (1997).

[53]Andrew C. Tam, Rev. Mod. Phys. **58**, 381 (1986).

[54]A. Hordvik and H. Schlossberg, Appl. Opt. **16**, 101 (1977).

[55]D. Ristau and J. Ebert, Appl. Opt. **25**, 4571 (1986).

[56]Antonios Seas, Constantinos Christofides and Mahendra Munidasa, Appl. Phys. Lett. **68** (4), 538 (1996).

[57]Goris L, Haenen K, Nesladek M, Wagner P, Vanderzande D, De Schepper L, D'Haen J, Lusten L and Manca J V, J. Mater. Sci. **40** (6), 1413 (2005).

[58]K. Rajasree, P. Radhakrishnan, V. P. N. Nampoori and C. P. G. Vallabhan, Meas. Sci. Technol. **4**, 591 (1993).

[59]Heiko Einsiedel, Sivia Mittler-Neher, Appl. Opt. **35** 270, 5406 (1996).

[60]M. A. Olmstead, N. M. Amer, S. Kohn, D Fournier, and A. C. Boccara, Appl. Phys. A **32**, 141 (1983).

[61]Andrew Skumanich, Mark Jurich, and J. D. Swalen, Appl. Phys. Lett. **62** (5), 446 (1993).

[62]J. H. Rohling, A. M. F. Caldeira, J. R. D. Pereira, A. N. Medina, A. C. Bento, M. L. Baesso, L. C. M. Miranda, and A. F. Rubira, J. Appl. Phys. **89** (4), 2220 (2001).

[63]Daniel Comeau, Alain Haché and Noureddine Melikechi, Appl. Phys. Lett. **83** (2), 246 (2003).

[64]J. H. Rohling, A. N. Medina, A. C. Bento, J. R. D. Pereira, A. F. Rubira, M. L. Baesso, and L.C. M. Miranda, J. Phys. D: Appl. Phys. **34** 407 (2001).

[65]J. H. Rohling, J. R. D. Pereira, A. N. Medina, A. C. Bento, M. L. Baesso, J. A. Sanpaio, S. M. Lima, and L.C. M. Miranda, Rev. Sci. Instrum. **74** (1), 291 (2003).

[66]Z. L. Wu, P. K. Kuo, Y.S. Lu, S. T. Gu, R. Krupka, Thin Solid Films, **290-291**, 271 (1996).

[67]Hu Haiyang, Fan Zhengxiu and liu Ye, Laser Phys. **10** (2), 633 (2000).

[68]E. Welsch, H. G. Walther, K. Freidrich and P. Echardt, J. Appl. Phys. **67**, 6575 (1990).

[69]R. T. Swimm and L. J. Hou, NIST Spec. Publ. **752**, 251 (1988).

[70]Z. L. Wu, Critical Rev. Opt. Sci. and Tech., **CR69,** 326 Proc. SPIE, (California, USA, 1997).

[71]W. B. Jackson, N. M. Amer, A.C. Boccara, and D. Fournier, Appl. Opt. **20**, 1333 (1981).

[72]L. Wei, Ph. D. Thesis, Department of Physics and Astronomy, Wayne State University (1993).

[73]A. Rosencwaig, J. Opsal, W. L. Smith, and D. L. Willenborg, Appl. Phys. Lett. **46**, 1013 (1985).

[74]D. Guidotti and H. M. van Driel, Appl. Phys. Lett. **47**, 1336 (1985).

[75]C. Christofides, I. A. Vitkin, and A Mandelis, J. Appl. Phys. **67**, 2815 (1990).

[76]A. Seas and C. Christofides, Appl. Phys. Lett. **66**. 3348 (1995).

[77]P. K. Kuo and M. Munidasa, Appl. Opt. **29** (36), 5326 (1990).

[78]Yuesheng Lu, P. K. Kuo, L. D. Favro, R. L. Thomas, Z. L. Wu, and S. T. Gu, Progress in Nat. Sci. **6**, S-202 (1996).

[79]R. Chow, J. R. Taylor, Z. L. Wu, R. Krupka, and T. Yang, "High reflectors absorptance measurements by surface thermal lensing technique", in *Laser-induced Damage in Optical Materials: 1996,* eds. H.E. Bennett, A.H. Guenther, M.R. Kozlowski, B.E. Newman and M.J. Soileau, SPIE Proc. **2966**, Bellingham (Washington, USA), 1997.

[80]H. Saito, M. Irikura, M. Haraguchi, and M. Fukui, Appl. Opt. **31**, 2047 (1992).

[81]Z. L. Wu, P. K. Kuo, Y. S. Lu, and S. T. Gu, Proc. SPIE **2714**, 294 (1996).

[82]P. K. Kuo, Y. X. Du, X. J. Shui and S. Y. Zhang, Progress in Nat. Sci. **6**, s-198 (1996).

[83]Y. Lu, P. K. Kuo, L.D. Favro, R. L. Thomas, Z. L. Wu, and S. T. Gu, Progress in Nat. Sci. **6**, s-202 (1996).

[84]M. A. Zambrano-Arjona, M. A. Smit, Juan J. Alvarado-Gil, Proc. SPIE **5776,** 471 (2005).

[85]W. D. Callister, Jr., *Materials Science and Engineering: An Introduction*, 5th ed. (Wiley, New York, 2000), p. 120.

[86] D. G. Legrand and J. T. Bendler, eds. *Handbook of Polycarbonate Science and Technology,* (Marcel Dekker, New York, 2000), p. 112.

[87] G. W. Ehrenstein, *Polymeric Materials: Structure- Properties- Applications*, (Hanser, Munich, 2001), p.169, 262.

[88] J. P. Gordon, R. C. C. Leite, R. S. Moore, S. P. S. Porto, and J. R. Whinnery, J. Appl. Phys. **36,** 3 (1965).

[89] C. Hu and J. R. Whinnery, Appl. Opt. **12,** 72 (1973).

[90] A. J. Twarowski and D. S. Kliger, Chem. Phys. **20,** 253 (1977).

[91] S. J. Sheldon, L. V. Knight, and J. M. Thorne, Appl. Opt. **21,** 1663 (1982).

[92]M. E. Long, R. L. Swofford, and A. C. Albrecht, Science **191,** 183 (1976).

[93]J. F. Power, Appl. Opt. **29**(1), 52 (1990).

[94]M. Thomsen and R. Gurung (private communication, 2005).

[95]M. Thomsen (private communication, 2005).

APPENDIX

The data presented in this report are saved in a CD named "Hussain" as well as on Laser lab computer model DELL XPS T500 located in the Laser Lab, Dept of Physics and Astronomy, Eastern Michigan University, Ypsilanti.

To access raw data, go to:

Hussain/raw data folder name/file name.

To access processed data, go to:

Hussain/FD plots/file name.

To access data for the time dependence runs presented in this work is stored under the folder named "Nandita."

The following table is shown to help retrieve data for each sample spot.

Table 1- Names of the folders and files to access data information for each sample spot presented in the thesis.

Sample Spot	Raw Data Folder	Raw Data Files	Processed Data Folder	Processed Data File	Log Book Reference
Spot 1	BH051904	BH051904A-Y	FD Plots	BH051904 B1 P36 FD	Book 01 Page 36
Spot 2	BH052604	BH052604A-Y	FD Plots	BH052604 B1 P44 FD	Book 01 Page 44
Spot 3	BH052904	BH052904A-Y	FD Plots	BH052904 B1 P52 FD	Book 01 Page 52
Spot 4	BH060604	BH060604A-Y	FD Plots	BH060604 B1 P61 FD	Book 01 Page 61
Spot 5	BH060904	BH060904A-Y	FD Plots	BH060904 B1 P67 FD	Book 01 Page 67
Spot 6	BH062404	BH062404A-Y	FD Plots	BH062404 B2 P13 FD	Book 02 Page 13
Spot 6 (re-run)	BH062904	BH062904A-Y	FD Plots	BH062904 B2 P16 FD	Book 02 Page 16
Outlier Spot	BH061204	BH061204A-Y	FD Plots	BH061204 B2 P01 FD	Book 02 Page 01